

PERKIN-ELMER

ELECTRO-OPTICAL DIVISION

NORWALK, CONNECTICUT

ENGINEERING REPORT NO. 8393

PHASE I REPORT
GIANT APERTURE TELESCOPE STUDY


DATE: MAY 12, 1966

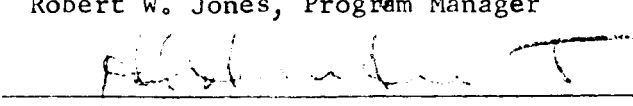
PREPARED FOR: CALIFORNIA INSTITUTE OF TECHNOLOGY

JET PROPULSION LABORATORY

4800 OAK GROVE DRIVE

PASADENA, CALIFORNIA


Robert W. Jones, Program Manager


Harold S. Hemstreet, Manager, Space Optics Department

Contributors:

R. Arguello
J. Buckley
R. Jones
J. Spalding
I. Steiner
W. Peters

TABLE OF CONTENTS

<u>Section</u>	<u>Title</u>	<u>Page</u>
I	INTRODUCTION	1
II	LASER DEEP-SPACE OPTICAL COMMUNICATION SYSTEM CONSIDERATIONS	4
	A. Laser Candidate and Detection Systems	4
	B. Selection of System Parameters	5
	C. Modulation Techniques	7
III	EFFECTS OF ATMOSPHERIC TURBULENCE ON OPTICAL SIGNALS	27
	A. General	27
	B. Coherence Diameter	28
	C. Calculation of $\int C_n^2 dx$	31
	D. Heterodyne Efficiency	35
	E. Scintillation	36
	F. Summary	41
IV	EFFECTS OF INCREASING ZENITH ANGLE ON OPTICAL SIGNALS	44
V	TELESCOPE CONFIGURATIONS FOR INCOHERENT DETECTION	48
	A. General	48
	B. Fixed Spherical Reflector	55
	C. Azimuth-Rotating Primary Mirror	76
	D. Conventional Telescope	82
VI	TELESCOPE CONFIGURATION FOR COHERENT DETECTION	84
	A. General	84
	B. Figure Accuracy	84
	C. Configuration	86
VII	CONCLUSIONS AND RECOMMENDATIONS	88

LIST OF ILLUSTRATIONS

<u>Figure</u>	<u>Title</u>	<u>Page</u>
1	Signal vs Noise for PCM/PL	12
2	Signal vs Noise for PPM	17
3	Scintillation vs Aperture	39
4	Detection Efficiency	40
5	The Celestial Sphere as Viewed by an Observer at Latitude L in the Northern Hemisphere	50
6	Sky Coverage Required to Assure Capability of Tracking an Object i_p out of Ecliptic Plane	52
7	Limiting Angles Associated with Sky Coverage Described by Figure 6.	53
8	Worst Case Angular Departure of a Planet From the Exliptic, as Seen From Earth	54
9	Telescope with Fixed Spherical Primary Mirror	57
10	Primary Mirror Surface Area vs f/No.	59
11	Mirror Configuration for Zodiac Coverage	60
12	Minimum Elevation Angle vs Primary Mirror f/No. For Various Degrees of Vignetting	62
13	Glass Requirements for Full Horizon Coverage	63
14	Fixed Dish + Movable Horizon Scanner	66
15	Tentative Optical Design	69
16	Field Angle Considerations for System with 20 arc-seconds Field Stop, 6 arc-seconds Blur Circle	71
17	Linear Approximation of Energy Collected vs Angle Off-axis	72

LIST OF ILLUSTRATIONS (Continued)

<u>Figure</u>	<u>Title</u>	<u>Page</u>
18	Telescope with Fixed Primary, Alt-azimuth Mounted Secondary Optics	74
19	Schematic of Azimuth Rotating Telescope	78
20	Azimuth Rotating Telescope	80

SECTION I

INTRODUCTION

This report presents the results of the first phase of a study aimed at reducing to practice the use of giant aperture telescopes as ground receivers for spacecraft communications.

The report considers two basic high data rate communication systems; one utilizing intensity detection, the other utilizing coherent or heterodyne detection.

It is unlikely that a single ground receiver, even with minor modifications, will be suitable for use with both techniques, because the larger aperture required for intensity detection will not have a good enough optical figure to permit coherent detection and the coherent system will not have a large enough aperture for use as an intensity detector.

We are then faced with making a system decision before proceeding with the construction of a ground station.

It is not the purpose of this study to investigate optical communication, a subject that has been treated extensively elsewhere (Refs. 1, thru 6). However, we have found it necessary to make a communications comparison of the two approaches in order to make meaningful recommendations concerning ground station requirements in terms of engineering feasibility, areas for further study or development, and cost.

Using the intensity detection technique, we can increase the data rate for a given spacecraft by increasing the diameter of the collecting aperture. There does not appear to be any limit to the aperture size other than cost.

Using coherent detection we gain data rate as we increase aperture only until we reach a certain limit imposed by the atmosphere. Increasing the aperture beyond this limit decreases the useful data rate.

We have studied the atmospheric effects and attempted to predict the maximum useful aperture diameter for coherent systems at several wavelengths.

Consideration has been given to several different mechanical configurations of the intensity detection receiver, all of which use the same basic optical system.

Consideration has also been given to the mechanical configuration of coherent systems but in less detail, since such a system could closely resemble a conventional astronomical telescope.

References

- 1 -- Determination of Optical Technology Experiments for a Satellite.
Perkin-Elmer, NASA CR-252, Contract NAS8-11408, July 1965.
- 2 -- Study for An Optical Technology Apollo Extension System.
Perkin-Elmer Report 8319, Contract NAS8-20255, April 1966.
- 3 -- Deep Space Optical Communications Study by Kenneth L. Brinkman,
NASA Contractor Report No. CR-73, Hughes Aircraft Company, El Segundo,
California, July 1964.
- 4 -- Investigation of Optical Spectral Regions for Space Communications.
ASTIA Document No. AD 410537, Ann Arbor: University of Michigan. May 1963.
- 5 -- Advanced Study on Optical Communications From Deep Space. Westinghouse
Electric Corporation, Baltimore, Maryland, Contract No. NAS9-2650,
August 1965.
- 6 -- Optical Space Communications System Study, General Electric. Philadelphia.
Pennsylvania. Contract No. NASw-540, Volumes I thru IV, February-March 1964.

SECTION II

LASER DEEP-SPACE OPTICAL
COMMUNICATION SYSTEM CONSIDERATIONS

We do not feel that a reasonable decision concerning the type of ground receiver to be used for a deep-space laser communication system can be made without a comparative analysis of the communications aspects of the various approaches. In this section these comparisons are made and conclusions drawn which permit a meaningful choice of aperture for the ground receiver.

A. LASER CANDIDATE AND DETECTION SYSTEMS

The following set of laser candidates and detection systems were evaluated and compared for use in a deep-space optical communication system:

Helium Neon - 6328\AA - Pulse Code Modulation with Polarization (PCM/PL)

Galium Arsenide - 8400\AA - Pulse Position Modulation (PPM)

Sun Pumped YAG - 1.06μ - Pulse Code Modulation with Polarization (PCM/PL)

Carbon Dioxide - 10.6μ - Coherent Detection, with Phase Shift Keying Subcarrier Modulation, (PSK)

We have not considered the 3.5μ region here because no laser of reasonable power output now exists and the development of such a laser seems unlikely. It would be meaningless to perform an analysis based on estimated powers and efficiencies of such a laser.

The wavelength dependent parameters which have been considered are:

1. Laser sources
2. Atmospheric transmission
3. Beam divergence
4. Energy per photon

5. Background
6. Detector response
7. Atmospheric turbulence effects
8. Optical efficiency
9. Predetection optical filter bandwidth and transmission.

Such factors as optical tolerances, pointing and alignment tolerances, which are also wavelength dependent, must also be considered in an evaluation of any particular system.

B. SELECTION OF SYSTEM PARAMETERS

All systems have been compared for a 10^8 and 1.5×10^8 statute mile deep-space to earth communication link for both day and night operation. From vehicle-earth station geometry considerations, it is assumed that the earth receiver tracks the space vehicle at a zenith angle of 60° . A constraint of constant reflector weight of 100 pounds was used to determine the vehicle transmitter aperture. Refer to Appendix C, Figure C-3, of NASA CR-252 for a reflector parameter chart of diffraction limited transmitter aperture diameter versus wavelength with reflector weight as a parameter. The transmitter aperture diameters for the HeNe, GaAs, and YAG wavelengths are all clustered near a 1 meter value.

The receiver aperture for the intensity detection techniques using HeNe, GaAs, or YAG was assumed to be the "photon bucket," (optical equivalent to the Arecibo microwave antenna). The receiver apertures for the coherent system are chosen on the basis of predicted daytime and nighttime atmospheric coherence diameters.

The earth-receiver field of view is governed predominantly by the inherent blur circle of the optical design, alignment and relative tilts between the optical segments, imperfections in the secondary optics, alignment of the secondary optics with primary mirror, telescope vibrations, and angle of arrival fluctuations caused by atmospheric turbulence. The value of 15 arc-seconds was chosen as a reasonable design value.

Transmitter and receiver optical transmittances of 50 percent are chosen on the basis of percentage obscuration of the secondary mirrors, losses incurred for air-to-glass interfaces, truncation of the intensity distribution output from the lasers, and reflectivity of the primary and secondary mirrors. It is interesting to note that techniques are available for mapping the laser intensity distribution into alternate distributions compatible with the transmitting optics.

The far field pattern of an unobscured circular aperture is the classical Airy pattern. Both the secondary obscuration and the non-uniform illumination of the transmitter aperture will distort the far-field distribution on the Earth. Both effects will decrease the width of the central maximum in the far field and will increase the energy contained in the side-lobes of the diffraction pattern. The energy contained outside the half power points of the far field pattern of the ideal uniformly illuminated aperture is 0.4.* A value of the beam distribution factor of 50 percent will be assumed as the loss in the far field at the optical system due to diffraction effects.

The scintillation factor for the large telescope aperture, "photon bucket," will be considered to be unity since there is considerable aperture averaging of atmospheric turbulence induced scintillation. The effect of scintillation for the coherent detection case has been discussed in another section of this report.

The selection of a very narrow optical predetection filter is dictated by the requirement for daylight communications in the presence of sky background. It may also be a necessity for nighttime communications if a planetary background (Mars) is considered.

The earth based receiver photomultiplier tubes used for the intensity detection systems considered will require cooling to limit dark current noise. It has been assumed that quantum efficiencies of photomultipliers

* Born and Wolf, Principles of Optics, p. 398. MacMillan Company, 1964.

have been enhanced by a factor of two by the technique of total internal reflection.* For coherent optical heterodyne communication, liquid helium cooled detectors can be employed to allow operation at the photon shot-noise limit at 10.6μ . This will require the detector to be suitably shielded from exchanging radiation with its environment except through the solid angle and the wavelength passband through which the signal must come. This means operation of the detector in a cooled reflecting shield, using a cooled narrow-passband filter over the signal aperture.

C. MODULATION TECHNIQUES

The deep-space optical communication system will be analyzed on the basis of 10^5 , 10^6 bit data rates with bit error probabilities of 10^{-3} . The modulation techniques considered are PCM/PL (Pulse Code Modulation with Polarized Light), PPM (Pulse Position Modulation), and coherent optical superheterodyne detection. Refer to the Interim Report to Marshall Space Flight Center for the "Study for an Optical Technology Apollo Extension System" (OTES) under contract NAS 8-20255, for a discussion of the advantages of each modulation technique.

1. PCM/PL at $\lambda = 6328\text{\AA}$

The number of photoelectrons per bit (N) generated at the photocathode is computed by substituting the numbers from Table I into the following equations:

$$N = \left[\frac{\lambda_c n \times 10^{25}}{2C} \right] \left[2P_d + \left(\frac{\pi}{4} a_r D_r \right)^2 \tau_a \tau_r \tau_f \lambda Q \right] \quad (1)$$

where Q , the background parameters, are given by:

$$Q_{\text{day sky}} = N_{\lambda B/a} \quad (2)$$

$$Q_{\text{Mars night}} = 0.4\pi H_{\lambda P/a_r}^2 \quad (3)$$

$$Q_{\text{stars}} = N_{\lambda s} \quad (4)$$

*Gunter, W.D., Erickson, E.F., Grant, G.R., "Enhancement of Photomultiplier Sensitivity by Total Internal Reflection," Applied Optics, Vol. 4, No. 4, April, 1965, p. 512.

TABLE I
COMMUNICATION PARAMETERS FOR SEVERAL WAVELENGTHS

Deep-Space to Earth Optical Communication Parameter	Symbol	Intensity Detection λ (Microns)		Coherent Detection	Comments and References
		0.6328	0.8400	λ 10.6 μ	
Transmitter Wavelength (m.)	λ_t	0.6328×10^{-6}	0.84×10^{-6}	1.06×10^{-6}	-
Predetection Optical Bandwidth (μ)	$\Delta\lambda$	0.125×10^{-4} 1.5×10^{-4}	5×10^{-3}	5×10^{-3}	For the Ne-He Laser two filters are considered: Lyot Polarization Filter, Spectrolab Filter. Re: NASA CR-252, interim report to Marshall Space Flight Center, "Study for an Optical Technology Apollo Extension System (OTES)," Contract NAS 8-20255
Quantum Efficiency (Photoelectrons/photon)	τ	0.16	7.2×10^{-3}	2×10^{-3}	Quantum Efficiencies based on "Enhancement of Photo-multiplier Sensitivity by Total Internal Reflection". Re: Applied Optics, Vol.4, April 1965, p. 512.
Information Data Rate (bits/sec)	C	10^5 10^6			Error Rate set at 10^{-3}
Diameter of Transmitter Aperture (m)	D_t	1	1	1	Refer to NASA CR-252, Appendix C, Figure C-3.
Diameter of Receiver Aperture (m)	D_r	10	10	10	Optical equivalent to Arecibo Microwave Antenna for intensity detection methods. Receiver aperture determined by predicted daytime and nighttime atmospheric coherence diameter for coherent detection.

TABLE I (Continued)

Deep-Space to Earth Optical Communication Parameter	Symbol	Intensity Detection λ (Microns)		Coherent Detection λ 10.6 μ	Comments and References
		0.6328	0.8400		
Receiver Field of View (rad.)	a_r	0.727x10 ⁻⁴		Single re-solution element of receiver	15 arc-second fov for intensity detection methods based on blur circle limitations of Earth receiver segments.
Range (statute miles)	R	10 ⁸ 1.5x10 ⁸			Re: NASA CR-252 Assumed rendezvous point of a minimum energy rendezvous trajectory (phase angle of 37.5°)
Receiver Optical Transmittance	τ_r	0.5			Re: P.E. Optical Technology Satellite Report, Phase II, p 5-3.
Predetection Optical Filter Transmission	τ_f	0.13 0.4	0.85	0.6	Re: 2nd row
Atmospheric Transmittance	τ_a	0.7	0.85	0.9	Assumed 60° zenith angle slant path.
Transmitter Optical Transmittance	τ_t	0.5			Re: P.E. Optical Technology Satellite Report, Phase II, p. 5-3.
Beam Distribution Factor	τ_d	0.5			Loss in intensity in far field due to diffraction effects.
Detector Type	-	RCA 7265 Photo-multiplier S-20 Surface	EMR543C Photo-multiplier S-1 Surface	RCA 7102 Photo-multiplier S-1 Surface	Re: NASA CR-252, and 3rd row
At Temperature	-	-70°C	-70°C	-70°C	Required Cooling to limit dark current.

TABLE I (Continued)

Deep-Space to Earth Optical Communication Parameter	Symbol	Intensity Detection $\frac{1}{\lambda} \rightarrow \frac{1}{\lambda} \leftarrow$ (Microns)			Coherent Detection λ	Comments and References
Noise Equivalent Power Input From Detector (watts)	P_D	0.6328	0.8400	1.06	λ 10.6 μ	Re: NASA CR-252, p. 7-34 Fig. 7-27 for photomulti- pliers 3rd row above. Santa Barbara Research Center Solid State Detectors.
Detectivity $\frac{1/2}{\text{watt}} \text{ (cps)}$	D^*	—	—	—	10^9	Re: Santa Barbara Research Center Solid State Detectors
Spectral Radiant Intensity of Sky (watts/m ² -ster- μ)	$N_{\lambda B}$	20	5	2.5	3.4	Re: NASA CR-252, p. 3-34, Table 3-5.
Spectral Irradiance from Mars (watts/m ² - μ)	$H_{\lambda P}$	3.5×10^{-8}	1.73×10^{-8}	0.92×10^{-8}	0.53×10^{-8}	Assumed rendezvous point of a minimum energy rendezvous trajectory Re: NASA CR-252, Fig. 7-17 p. 7-26.
Spectral Radiant Intensity of Star Field (watts/m ² -ster- μ)	$N_{\lambda S}$	3.3×10^{-6}	1.5×10^{-6}	1.15×10^{-6}	9.8×10^{-10}	NASA CR-252, Fig. 7-14, p. 7-23.
Transmitter Optical Power (watts)	P_T	1	—	—	—	All transmitter optical power calculations are normalized for a value of 1 watt.

The signal in (pe/bit) required for a bit error rate of 10^{-3} , (i.e., 1 per 1000) in the presence of the noise given by Equation (1) can be determined from Figure 1.* The transmitted light power needed to maintain a 10^{-3} bit error probability is obtained by dividing the corresponding required signal in (pe/bit) obtained from Figure 1 by the available signal (S) in (pe/bit) per watt of transmitted light power given by Equation (5).

$$S(\text{pe/bit}) = \frac{\lambda_t \eta \times 10^{25}}{2C} \left[\frac{D_t D_r}{1963 \lambda_t R} \right]^2 \tau_r \tau_f \tau_a \tau_t \tau_d P_t \quad (5)$$

$$(1.22 \times 1609 \frac{\text{m}}{\text{n.m.}} = 1963)$$

Substituting appropriate numbers for $\lambda = 6328\text{\AA}$ from Table I, Equations (1) through (5) become:

$$N(\text{pe/bit}) = \frac{506}{C} \left[2 + 11.56 \times 10^7 \tau_f \lambda Q \right] \quad (6)$$

$$Q_{\text{day sky}} = 28.6 \quad (7)$$

$$Q_{\text{Mars night}} = 8.32 \quad (8)$$

$$Q_{\text{stars}} = 3.3 \times 10^{-6} \quad (9)$$

$$S(\text{pe/bit}) = 2.87 \times 10^{24} \left(\frac{\tau_f}{CR^2} \right) \quad (10)$$

Table II gives background noise, required signal, and required transmitted power for a 10^{-3} bit error rate and different values of channel capacity (C), operating range (R), and different predetection optical filters.

6.3 photoelectrons per bit is the signal required for a 10^{-3} bit error rate when the background noise is zero. It is therefore evident from Table II that the average star background is a negligible source of noise even when the broad optical bandwidth Spectrolab filter is used. The use of narrow band optical filters at night against an average star background is therefore not recommended. Its relatively low transmittance would only increase the signal's attenuation, thus necessitating an increase in the transmitted signal power.

*Peters, W. W. Pulse Position Optical Communication System, NATCOM Proceedings, 1964

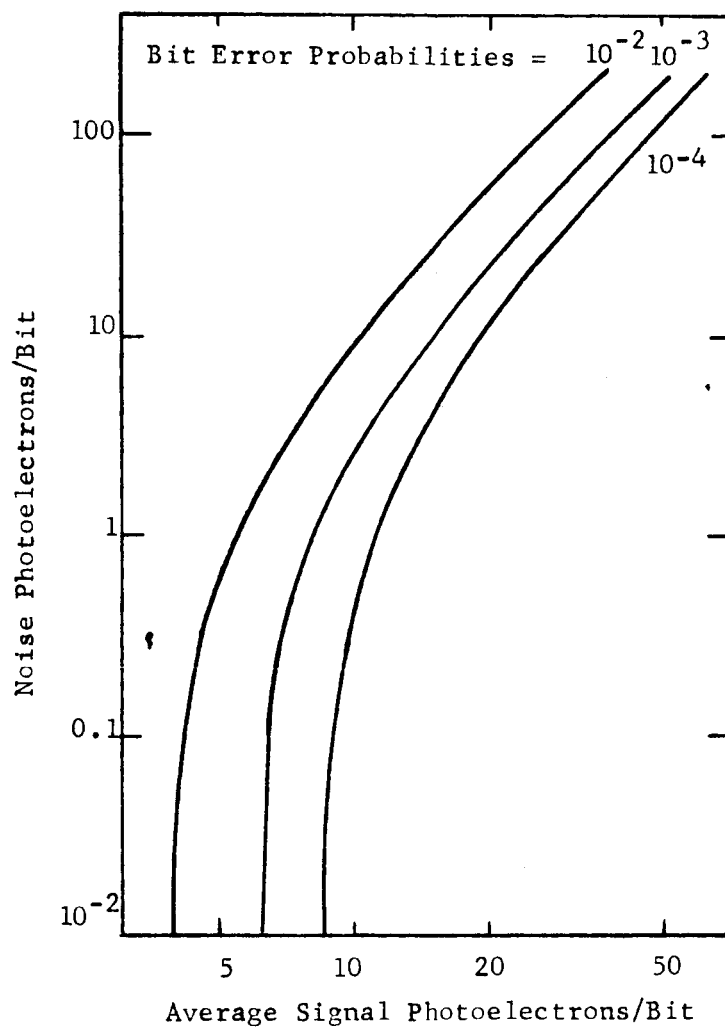


Figure 1. Signal vs Noise for PCM/PL

With Mars in the field of view at night or with the sky background during the day, the use of the narrow band Lyot optical filter requires less signal than the Spectrolab filter (see Table II), thus proving that the day sky and Mars are formidable noise sources.

The transmitted signal power required is directly proportional to both the required signal and the channel capacity. In the case where the background noise is negligible (see average star background in Table II), the transmitted signal power is only proportional to channel capacity. For other background sources the increase in noise due to decreasing channel capacity increases the required signal. However, the required transmitted signal power still diminishes with decreasing channel capacity in spite of an increasing noise level.

2. PPM at $\lambda = 8400\text{\AA}$

Equations (1) through (5) which were presented for PCM/PL at $\lambda = 6328\text{\AA}$ can be modified to apply also to PPM at $\lambda = 8400\text{\AA}$ by multiplying Equations (1) and (5) by the factor $1/2^Q$, where Q is the number of slots per pulse in PPM. This expresses the noise (N) and the received signal (S) in units of photoelectrons per slot, rather than in units of photoelectrons per bit.

Note that in the case of PPM, P_t denotes average optical power transmitted, i.e., total energy per word (Q slots) divided by the word time interval. In the case of PCM/PL, P_t also denotes average optical power transmitted, but in a CW operational mode.

Substitution of appropriate values for $\lambda = 8400\text{\AA}$ from Table I into the properly modified Equations (1) through (5) yields the following Equations:

$$N(\text{pe/slot}) = \frac{302.5Q}{2^Q C} \left[1.1 + 703Q \right] \quad (11)$$

$$Q_{\text{day sky}} = 5.88 \quad (12)$$

$$Q_{\text{Mars night}} = 4.11 \quad (13)$$

$$Q_{\text{stars}} = 1.5 \times 10^{-6} \quad (14)$$

$$S(\text{pe/slot}) = \frac{5.91 \gamma \times 10^{22}}{CR^2} \quad (15)$$

where α is the number of slots per PPM pulse.

Table III gives the background noise, required signal, and required transmitted optical power for a 10^{-3} bit error rate and for different values of channel capacity (C), number of slots per pulse (α), and operating range (R). The required signal for a 10^{-3} bit error rate was computed from Figure 2.*

As in the preceding cases, the average star background is a negligible noise source, and the day sky and Mars are formidable noise sources. Similarly, as before, the required signal power diminishes with decreasing channel capacity.

The values of α chosen in Table III are based on estimated reasonable combinations of pulse repetition rates and pulse durations which may be available in the future. For example, at 10^6 bits/sec and 5 slots per pulse, the pulse repetition rate is 2×10^5 pulses per second and the pulse duration is 156 nanoseconds. At 10^5 bits/sec and 9 slots per pulse, the pulse repetition rate is 1.1×10^4 pulses per second and the pulse duration is 176 nanoseconds.

3. PCM/PL at $\lambda = 10600\text{\AA}$

Equations (1) through (5) which were presented for PCM/PL at $\lambda = 6328\text{\AA}$ apply also for PCM/PL at $\lambda = 10600\text{\AA}$. Substitution of the appropriate numbers for $\lambda = 10600\text{\AA}$ from Table I into Equations (1) through (5) yields the following equations:

*Peters, W. W. Pulse Position Optical Communication System, NATCOM Proceedings, 1964.

Table III. Link Parameters 8400A PPM

BACKGROUND SOURCE	DAY SKY		MARS NIGHT		STARS (AVERAGE)	
Background Noise (N) pe/slot	16.58	18.7	11.8	13.3	Negligible	Negligible
Required Signal (pe/slot) for a 10^{-3} bit error rate	23.5	30	23	29.5	6.3	
Required Transmitter Optical Power (watts)	0.566	1.27	0.033	0.075	0.125	0.007
Channel Capacity (bits/sec) and number of slots/pulse	$C=10^6$ $\alpha=5$	$C=10^5$ $\alpha=9$	$C=10^6$ $\alpha=5$	$C=10^5$ $\alpha=9$	$C=10^6$ $\alpha=5$	$C=10^5$ $\alpha=9$
Operating Range (R) statute miles	10^8	1.5×10^8	10^8	1.5×10^8	10^8	1.5×10^8
Predetection Optical Filter	$\Delta\lambda = 50\text{\AA}$ $T_f = 0.85$					

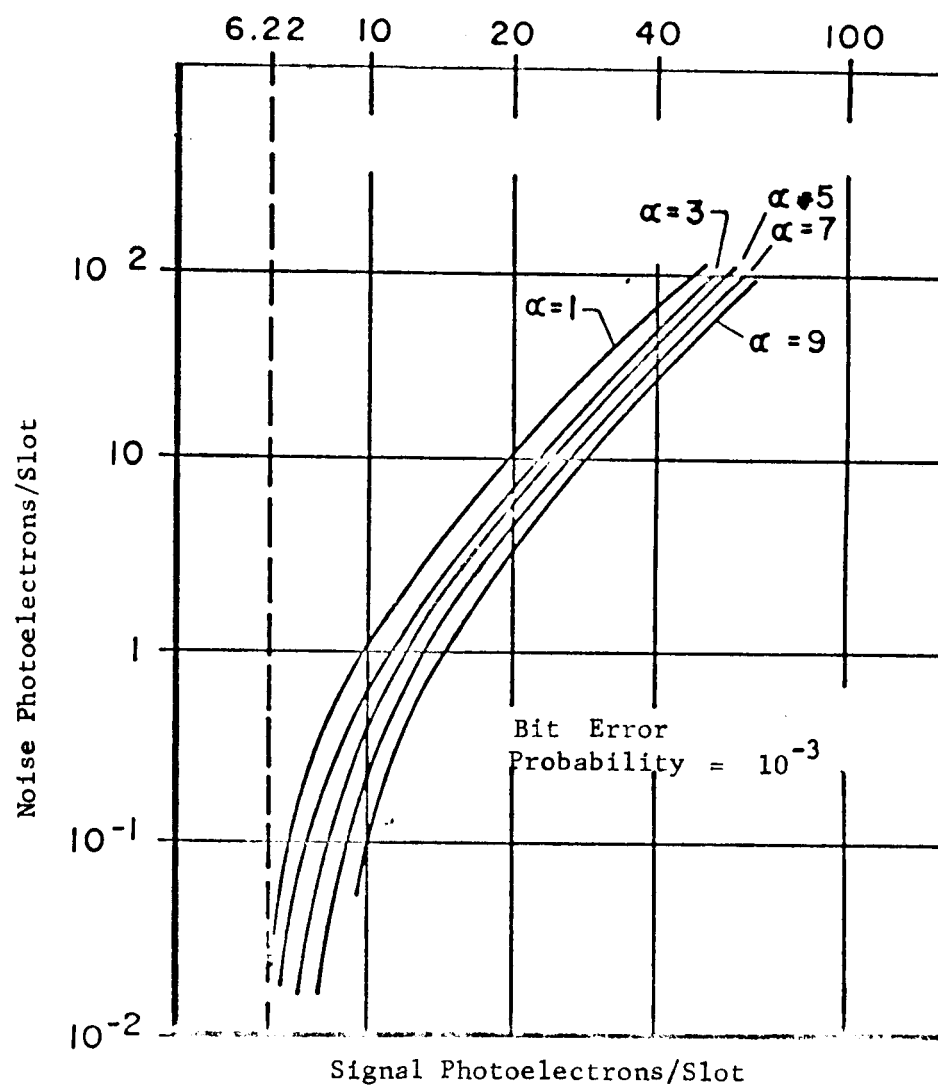


Figure 2. Signal vs Noise for PPM

$$N(\text{pe/bit}) = \frac{106}{C} [1 + 44,600Q] \quad (16)$$

$$Q_{\text{day sky}} = 2.78 \quad (17)$$

$$Q_{\text{Mars night}} = 2.18 \quad (18)$$

$$Q_{\text{stars}} = 1.2 \times 10^{-6} \quad (19)$$

$$S(\text{pe/bit}) = 1.65 \times 10^{22} \left[\frac{1}{CR^2} \right] \quad (20)$$

Table IV gives the background noise, required signal, and required transmitted optical power for a 10^{-3} bit error probability and for different values of channel capacity (C) and operating range (R). The required signal for a 10^{-3} bit error probability was computed from Figure 1.

As in the $\lambda = 6328\text{\AA}$ case, the average star background is a negligible noise source, and the day sky and Mars are formidable noise sources. Similarly, as in the $\lambda = 6328\text{\AA}$ case, the required transmitted signal power diminishes with decreasing channel capacity.

4. Optical Heterodyne Detection

This demodulation technique requires that the optical signal be heterodyned with an optical local oscillator signal on the surface of a photodetector. For a high detection efficiency, the phase fronts of the signal and optical local oscillator must "match" to within less than a half wavelength over the detected wavefront. The random fluctuations of phase caused by atmospheric turbulence will limit the useful aperture of a receiver. However, the advantages of coherent detection are significant. The background noise bandwidth is not determined by the optical predetection filter, but by the bandwidth of the post detection amplifiers. Therefore, the noise and signal bandwidths will be equal. Only the background radiation from one resolution element of the field of view of the receiver telescope will be in phase with the local oscillator signal. Therefore, a coherent optical receiver has the capability of operating in a very high background noise environment because of

Table IV. Link Parameters 10.600A PCM/PL

BACKGROUND SOURCE	DAY SKY		MARS (NIGHT)		STARS (AVERAGE)		
Background Noise (N) pe/bit	13.2	132	10.3	103	112×10^{-6}		
Required Signal (pe/bit) for a 10^{-3} bit error rate	16.5	41	15	37	6.3		
Required Transmitter Optical Power (watts)	10	23	2.5	5.6	20	5	0.83
Channel Capacity (C) (bits/sec)	10^6	10^5	10^6	10^5	10^6	10^5	10^5
Operating Range (R) (statute Miles)	10^8	1.5×10^8	10^8	1.5×10^8	10^8	1.5×10^8	10^8 1.5×10^8
Predetection Optical Filter	$\Delta\lambda = 50\text{\AA}$ and $\tau_f = 0.6$						

its noise suppression capabilities. In addition, heterodyne detection affords conversion gain. The received optical signal is of very low power. Without conversion gain, amplifiers immediately following the detector would not have sensitivity to noiselessly amplify the signal. However, the conversion gain of the coherent detection process increases the amplitude of the detector output and thus allows noise-free post detection amplification.

In order to compare the achievable data rate for a deep-space coherent optical detection system with an intensity detection technique, we will assume that the subcarrier detector requires a 10db signal-to-noise ratio. In considering coherent detection, the dominant noise sources are the background energy from one resolution element of the field of view of the receiver telescope and the noise introduced by the local oscillator. Refer to section I-3.2.4 of Perkin-Elmer Interim Report to Marshall Space Flight Center on "Study for an Optical Technology Apollo Extension System (OTES)," Contract NAS 8-20255, for a derivation of the signal-to-noise ratio obtained at the intermediate frequency amplifiers. We will assume that the local oscillator noise power in the signal bandwidth B can be made quite negligible with respect to other noise sources. Then

$$SNR = \frac{\eta}{h\nu B} \left[\frac{P_s}{1 + \frac{P_o B}{h\nu B}} \right]$$

where:

- SNR = signal-to-noise ratio at output of intermediate frequency amplifiers
- η = Planck's constant quantum efficiency of detection
- ν = optical frequency
- P_s = signal power incident on detector
- B = signal bandwidth
- $P_o B$ = background noise spectral intensity contained in one resolution element of the receiver optics as seen through signal bandwidth B.

The above equation is valid provided that the local oscillator power is:

$$P_{Lo} \gg \frac{P_s + P_{oB} + P_{NoB} + P_{No} + P_{Dc}}{1 + \frac{r}{h\nu B} [P_{oB} + P_{NoB}]} \quad (21)$$

where

- P_{Lo} = local oscillator power in single mode
- P_{oB} = background noise spectral intensity contained in one resolution element of the receiver optics as seen through an optical filter of bandwidth B_o
- P_{NoB} = local oscillator noise power in the signal bandwidth B
- P_{No} = local noise power in the signal bandwidth B
- P_{Dc} = incident power equivalent to the dark current

The other parameters are as defined previously.

If we assume that the signal power is of sufficient magnitude and that the post detection amplifiers insert no additional noise, then the above equations may be used to obtain the data rate and bit error rates. The signal bandwidth is assumed to be equal to ten times the data rate. Sub-carrier modulation techniques such as PSK (phase shift keying), have bit error rates of 10^{-3} when the SNR at subcarrier detection is 10db. Similar assumption on bit error rate is invoked for the 10.6μ coherent system.

5. Communication Link Calculations

Refer to Table I for a summary listing of system parameters for the deep-space coherent detection link.

The signal photon arrival rate incident on the detector, $P_s/h\nu$ per watt of transmitted optical power P_t is equal to:

$$\frac{P_s}{h\nu P_t} = \left[\text{Power Density Incident on Detector} \right] \frac{\lambda}{hc} \frac{\pi D_r^2}{4} \tau_t \tau_d \tau_a \tau_r \tau_f$$

where all parameters are defined in Table I. The pertinent background power P_{OB} is that obtained from day sky, Mars, average star field, contained in one resolution element of the receiver optics as seen through the signal bandwidth B .

In order to establish local oscillator power requirements it is necessary to compute the noise equivalent power P_{Dc} of the solid state detector; then

$$P_{Dc} = \sqrt{AB/D^*}$$

where A is the area of the detector equal to $(0.3\text{mm})^2 = 9 \times 10^{-8} \text{ cm}^2$ and B is the i.f. bandwidth equal to 1 and 10 mc/s, for data rates 10^5 and 10^6 bits per second respectively. D^* is the detectivity of the detector equal to $10^{11} \text{ cm}^2 \text{ cps/watt}$.

In order to achieve the SNR performance given above, the local oscillator power must be such that the local oscillator shot noise predominates over the other components of shot noise. However, the local oscillator power must be less than what is necessary to saturate the detector. A local oscillator of 20 μ watts will probably meet both conditions for the cases listed in Table V.

Refer to Table V for a listing of the performance characteristics of the 10.6 μ CO_2 laser communication system for several cases of interest.

D. CONCLUSIONS

Table VI presents pertinent properties of several lasers that are candidates for transmitters in a deep-space optical communication link. The entries in Table VI are current estimates and are subject to change as laser technology advances. We shall compare the estimated output optical powers from Table VI with the output optical powers required, which are given in Tables II through V.

TABLE V
LINK PARAMETERS CO₂ - 10.6μ COHERENT DETECTION SYSTEM

Background Source		Day Sky		Day Sky Plus Mars		Stars (ave)		Mars (Night)	
Background Noise Spectral Intensity in watts contained in one resolution element of the receiver optics as seen through signal bandwidth B, (BP ₀)	2.1x10 ⁻¹⁵	2.1x10 ⁻¹⁴	2.6x10 ⁻¹⁴	2.6x10 ⁻¹⁴	6.1x10 ⁻²⁵	6.1x10 ⁻²⁴	5x10 ⁻¹⁶	5x10 ⁻¹⁵	
					(negligible)				
Required Signal Power P _s incident on detector in watts for bit error rate of 10 ⁻³ , SNR = 10db	9.6x10 ⁻¹³	9.6x10 ⁻¹²	9.8x10 ⁻¹³	9.8x10 ⁻¹²	9.5x10 ⁻¹³	9.5x10 ⁻¹²	9.6x10 ⁻¹³	9.6x10 ⁻¹²	
Required Transmitter Optical Power (watts)	8.35	83.5	19.2	192	2.06	20.6	4.63	46.3	
Channel capacity (C), (Bits/Sec)	10 ⁵	10 ⁶	10 ⁵	10 ⁶	10 ⁵	10 ⁶	10 ⁵	10 ⁶	
Receiver Aperture (D _r), (Meters)	2	2	2	2	4	4	4	4	
Operating Range (R), (Statute Miles)	10 ⁸	1.5x10 ⁸	1.5x10 ⁸	1.5x10 ⁸	10 ⁸	10 ⁸	1.5x10 ⁸	1.5x10 ⁸	
Quantum Efficiency = 0.2									

Table VI. 1966 Laser Comparisons

PARAMETER	HE:NE	Ga As	Sun Pumped Yag	CO ₂
Output/Optical power	Moderate (1/4 watt)	>1 W	~10W	Very high (Possibly 1KW)
Efficiency (well above threshold)	Poor (10^{-4} - 10^{-3})	0.5	<0.01	Very Good 0.1 - 0.4
Detectability	Good	Poor	Poor	Good (For coherent detection)
Reliability (remote)	Good	Good	Unknown	Good
Size	Moderate	Minute	Needs Bulky Solar Collector	Large
Life	Long (>500hr)	Long	Long	Long
Cost	Moderate	Cheap	High	Low
Biggest Problem	Limited/Power	Mode & Wave-length Uncertainties	Heat Dissipation	Flowing Gas

In the case of the 6328A, He-Ne (PCM/PL) Laser System, (operated at the data rate of 10^6 bits/sec), the laser output power needed varies from 600 mw, (at an operating range of 1.5×10^8 statute miles, and using the Lyot filter in the presence of day sky background), to 55 mw, (at an operating range of 10^8 statute miles, and using the Spectrolab filter in the presence of an average nighttime star field background). An optimistic estimate of the output optical power available from the He-Ne laser is 250 milliwatts. It is therefore probable that a 10^6 bit/sec data rate can be achieved only in the presence of the average nighttime star field background (where the maximum required laser output optical power from Table II is 120 mw). In the presence of a day sky or night Mars background, the required laser output optical power from Table II exceeds the estimated 250 milliwatts power available. When the data rate is reduced from 10^6 bits/second to 10^5 bits/second, 250 milliwatts estimated available power exceeds the powers required under any background condition considered in Table II (the maximum requirement being 200 milliwatts at a range of 1.5×10^8 statute miles, and using the Spectrolab filter against a day sky background).

In the case of the 1.06μ sun pumped YAG (PCM/PL) laser system (operated at data rate of 10^6 bits/sec), the laser output optical power needed varies from 23 watts (at an operating range of 1.5×10^8 statute miles, in the presence of day sky background) to 3.8 watts (at an operating range of 10^8 statute miles in the presence of the average nighttime star field background). An estimate of the output optical power available from the YAG laser is approximately 10 watts. According to Table IV, ten watts of available laser optical output power is sufficient for the establishment of the communication link at a data rate of 10^6 bits/sec in the presence of nighttime average star field background or in the presence of a day sky background at a range of 10^8 statute miles. Reduction of the data rate to 10^5 bits/sec will reduce the required laser optical output power below the ten watt available level for all background conditions considered in Table IV.

In the case of the 8400Å GaAs laser system, (PPM), (operated at a data rate of 10^6 bits/sec), in accordance with Table III, the required laser output optical power varies from 1.27w average (at an operating range of 1.5×10^8 statute miles, in the presence of day sky background) to 7mw (at a range of 10^8 statute miles in the presence of the average nighttime star field background). The output optical power available from the GaAs laser is estimated to exceed 1 watt. This power equals or exceeds requirements for the establishment of the communication link under all conditions of Table III except for 1.27w requirement above.

In the case of the 10.6μ coherent laser system, operated at a data rate of 10^6 bits/sec, the required laser output optical powers varies from 192 watts (at a range of 1.5×10^8 statute miles, in the presence of day sky plus Mars background) to 20.6 watts (at a range of 10^8 statute miles in the presence of the nighttime average star field background). Although a 1 kw CO₂ laser may be achievable for an Earth-bound laser, the feasibility of a 192 watt spaceborne laser system should be further investigated from the viewpoint of weight and bulk. Communication at the reduced data rate of 10^5 bits/sec appears quite feasible, since the output optical power requirements are reduced, ranging from 19.2 watts (at a range of 1.5×10^8 statute miles against a day sky plus Mars background) to 2 watts (at a range of 10^8 statute miles against a nighttime average star field background).

SECTION III

EFFECTS OF ATMOSPHERIC TURBULENCE
ON OPTICAL SIGNALS

A. GENERAL

In this section we will estimate the effects of atmospheric turbulence on heterodyne and on amplitude sensitive detectors. To this end we will calculate the losses of a heterodyne system as a function of aperture, due to superimposed phase fluctuation, and also the amplitude fluctuations caused by atmospheric turbulence. Having made these calculations we will in the last section make some comparisons of the two types of system.

The analysis depends heavily on the following references:

1. Fried, David: The Statistics of a Geometric Interpretation of Wavefront Distortion, Tech. Memo 172, E-O Lab., No. American Aviation Inc., Space and Information Systems Div., Torrance, California
2. Fried, David: Optical Heterodyne Detection of an Atmospherically Distorted Signal Wavefront, Tech Memo 118, E-O Lab, No. American Aviation Inc., Space and Information Systems Div., Torrance, California, July 1964
3. Gardner: Some Effects of Atmospheric Turbulence on Optical Heterodyne Communications, IEEE International Convention, 1964
4. Goldstein: et al, Heterodyne Measurements of Light Propagation Through Atmospheric Turbulence, Proc. IEEE, p. 1172, Sept. 1965
5. Tatarski: Wave Propagation in a Turbulent Medium. McGraw Hill, 1961
6. Hufnagel, R.E. and N.R. Stanley, Image Transmission Through Turbulent Media, JOSA, Vol. 54, p. 52, 1964.

B. COHERENCE DIAMETER

Tatarski has derived the phase structure function $D_\phi(r)$ for a plane wave, assuming homogeneous isotropic turbulence and the 2/3 law for turbulence. This is usually given as*

$$D_\phi(r) = \langle (\phi(r_1) - \phi(r_2))^2 \rangle = 2.91 k^2 L C_n^2 r^{5/3} \text{ for horizontal path which is valid for } r \geq \sqrt{\lambda} L. \text{ For } r \leq \sqrt{\lambda} L$$

$$D_\phi(r) = 1.46 k^2 L C_n^2 r^{5/3}$$

These all assume $r \geq \ell_0$. A more general form is

$$D_\phi(r) = 2.91 k^2 L C_n^2 r^{5/3} - 0.62 C_n^2 L^{11/6} k^2 [1 - b_A(r)]$$

which is valid for all $r \gg \ell_0$. In most cases the last term is negligible.

For $r < \ell_0$ we would have

$$\begin{aligned} D_\phi(r) &= 3.44 k^2 L C_n^2 \ell_0^{-1/3} r^2 - 1.72 C_n^2 k^2 L \ell_0^{-1/3} r^2 \\ &= 1.72 k^2 L C_n^2 \ell_0^{-1/3} r^2 \end{aligned}$$

In general ℓ_0 is of the order of 5mm near the ground, so we may neglect this formulation. The change of form from $r \geq \sqrt{\lambda} L$ to $r \leq \sqrt{\lambda} L$ is uniform, and thus there is a 2:1 change in $D_\phi(r)$, which occurs in the region near $r \simeq \sqrt{\lambda} L$, but which is not abrupt. If the atmosphere is not uniform, $C_n^2 L$ must be replaced with the integral $\int C_n^2 dx$ taken over the path. Thus we may use as our basic structure function

$$\begin{aligned} D_{\phi_f} &= 1.46 k^2 r^{5/3} \int C_n^2 dx & r \leq \sqrt{\lambda} L \\ D_{\phi_r} &= 2 D_{\phi_f} & r \geq \sqrt{\lambda} L \end{aligned}$$

*For Definition of Symbols, refer to Page 38.

using the CGS system, we see that $\sqrt{\lambda}L$ in the visible is of the order of 10cm. For 1μ radiation this would become 14cm, for 3μ , 24.5cm, for 10μ , 45cm, and for 20μ , 63cm. These are for a path through the entire atmosphere and are given only approximately.

For short path lengths, of the order of a few kilometers, and moderate ρ , we see that the second form should be used.

An analysis by Fried shows that for a phase structure function of the form $D_\phi = a\rho^{5/3}$ the deviation of phase over an aperture can be given by

$$\langle \Delta_c \rangle = 1.013 \left(D/r_o \right)^{5/3}$$

$$\langle \Delta_L \rangle = 0.1301 \left(D/r_o \right)^{5/3}$$

$$\langle \Delta_s \rangle = 0.109 \left(D/r_o \right)^{5/3}$$

$$\langle \Delta_Q \rangle = 0.0630 \left(D/r_o \right)^{5/3}$$

where Δ_c is the phase fluctuation with no phase front correction.

Δ_L includes correcting for tilt (i.e., image tracking), Δ_s includes correcting for the focus in addition to tracking, and Δ_Q includes a quadratic correction.

r_o is a value that he defines as $\left(\frac{6.88}{a} \right)^{3/5}$. Fried then further specializes his formulation, giving D_j^* as the diameter for which $\langle \Delta_j \rangle$ equals some value D^* . These are as follows:

$$D_o^* = 0.992 r_o (\Delta^*)^{3/5}$$

$$D_L^* = 3.40 r_o (\Delta^*)^{3/5}$$

$$D_s^* = 3.79 r_o (\Delta^*)^{3/5}$$

$$D_Q^* = 5.26 r_o (\Delta^*)^{3/5}$$

Thus with no correction, and letting $\Delta^* = 1$, we have approximately

$$D_c \sim r_o,$$

so that r_o is the diameter for which phase shifts of one radian occur. This corresponds closely to Goldstein's D_{eff} , and may be given as

$$r_o \sim D_{eff} \sim 0.46 \lambda^{6/5} \left(\int C_n^2 dx \right)^{-3/5} \quad \rho \geq \sqrt{\lambda L}$$

or, for $\rho \leq \sqrt{\lambda L}$,

$$\begin{aligned} r_o \sim D_{eff} &\sim 0.46 \lambda^{6/5} \left(\int C_n^2 dx \right)^{-3/5} \quad 2^{3/5} \\ &= 0.7 \lambda^{6/5} (C_n^2 dx)^{-3/5} \quad \rho \leq \sqrt{\lambda L} \end{aligned}$$

We may regard Fried's r_o , or Goldstein's D_{eff} as a sort of coherence diameter.

We note further that if the image is tracked, it is possible to increase r_o by a factor of 3.4, further gains being possible, but difficult to instrument.

An intuitive estimate of r_o can be made considering the seeing image of a star, which is usually (at night) of the order of a second of arc. This is the same size as would be given by roughly a 10cm aperture, so that for nighttime observations we estimate r_o in the visible to be of the order of 10cm.

Before proceeding further we see that it is necessary to estimate $\int C_n^2 dx$, which will be done in the next section.

C. CALCULATION OF $\int C_n^2 dx$

The key to any calculation is the integral $\int C_n^2 dx$, taken along the path of the light through the atmosphere. C_n is of course a highly variable quantity, varying with height, surface conditions, time of day, and general meteorological conditions. Thus any calculation must be approximate.

Several points in a calculation are evident however. In any upward looking cases the value of the integral is set to at least one significant figure by the first one hundred meters of atmosphere above the observer. Changes through the day will change this significant figure, so there is little point in integrating past the first hundred meters. Further, we may assume that the instrument is a few meters above the ground, so that we need not include the immediate surface effects.

As the elevation of a station is changed, this first hundred meters is dominated by ground effects. In the daytime the dominant factor is thermal input to the ground, and although the density goes down with increasing altitude, the thermal content of the air decreases also, causing larger temperature fluctuations for the same input. As a result C_n will not decrease by a large amount as altitude is increased. Actually this corresponds to experience - seeing improves with altitude of an observatory but nowhere near as radically as might be expected from the free air value of C_n . A good site at a few thousand feet is only two or three times worse than a good site at five or six thousand feet.

We must note that the seeing at a site is strongly affected by local conditions, and at night by the presence or absence of an inversion layer, and the amount of mixing of local air due to the wind. In this context we should also remember that seeing at night, with the presence of an inversion layer, deviates from that of a simple turbulence theory, and in many cases the 2/3 law is violated. This is of course more true at night than in the daytime, and depends on many local factors.

To evaluate $\int C_n^2 dx$ we may use either Fried's formula,

$$C_n^2 = A L_o^{-2/3}$$

where $A = 6.7 \times 10^{-14} \exp(-h/3200)$, $L_o = 2h^{1/2}$

or Hufnagel's empirical curves. Both of these agree fairly well, although Fried's values are slightly lower than Hufnagel's. Also, Goldstein has measured values over an approximately horizontal path, showing the variation as a function of the time of day. These values correspond roughly to those of Fried and Hufnagel for a height of approximately thirty meters, the agreement depending on the time of day one assumes for Fried and Hufnagel. Goldstein's light path was one that would accentuate the effects of air currents ascending the side of the mountain, so it undoubtedly gives a pessimistic value for the middle of the night, or for the optimum.

Using Hufnagel's curves modified by Goldstein's measurements and numerically integrating, we can arrive at the following values for $\int C_n^2 dx$, assuming a vertical path. For a slant path it is only necessary to multiply by the secant of the zenith distance.

$\int C_n^2 dx$ (vertical)				
Noon	Afternoon	Twilight	Night	Hufnagel
2.2×10^{-11}	7×10^{-11}	7×10^{-12}	1.5×10^{-11}	2.2×10^{-11}
$\left(\int C_n^2 dx \right)^{-3/5}$				
(2.5×10^6)	(1.25×10^6)	(5×10^6)	(3.1×10^6)	(2.5×10^6)
$\lambda^{6/5} = \lambda^{1.2}$				
$0.6\mu = 0.6 \times 10^{-4}$ cm			0.085×10^{-4}	
$1\mu = 1 \times 10^{-4}$ cm			0.158×10^{-4}	
$4\mu = 4 \times 10^{-4}$ cm			0.835×10^{-4}	
$10\mu = 10 \times 10^{-4}$ cm			2.81×10^{-4}	
$20\mu = 20 \times 10^{-4}$ cm			5.7×10^{-4}	

We have tabulated, for comparison purposes, values that use Goldstein's variation through a day; Hufnagel's curve, unmodified; and Fried's values. All data has been rounded to two significant figures. The integration ignores the first five meters above the ground.

TABLE VII
TABULATION OF D_{eff} in CENTIMETERS
where $D_{\text{eff}} = 4.6 \lambda^{6/5} \left(\int C_n^2 dx \right)^{3/5}$

λ, μ	Morning	Afternoon	Twilight	Night	Hufnagel	Fried Night - Day	
0.6	9.8	4.9	20	12	9.8	7.2	3.6
1	18	9.0	36	22	18	13	6.6
4	95	48	190	120	96	70	35
10	320	160	640	400	320	210	100
20	660	330	1300	810	660	490	250

TABLE VII (Continued)

D _{eff} Corrected for Tracking (Multiply by 3.4)							
λ, μ	Morning	Afternoon	Twilight	Night	Hufnagel	Fried Night - Day	
0.6	33.5	16.7	68	4.07	33.5	24.5	12.3
1	61	30.7	123	745	61	44	22.5
4	324	163	645	407	327	238	119
10	1090	542	2180	1360	1090	712	340
20	2240	1120	4420	2760	2240	1660	850

D _{eff} Corrected for Zenith Distance of 60° (Multiply by 0.66)							
0.6	6.45	3.22	13.2	7.9	6.45	4.75	2.37
1	11.8	5.9	23.6	14.5	11.8	8.5	4.34
4	62.5	31.6	124	79	63	46	23
10	210	105	420	264	210	138	66
20	435	217	855	530	435	322	164

D _{eff} Corrected for 60° and Tracking (Multiply by 2.24)							
0.6	22	11	45	27	22	15.9	8.05
1	40.5	20.1	80.5	49.4	405	29.2	14.8
4	213	107	426	269	214	157	78.5
10	719	359	1430	895	718	471	224
20	1480	740	2920	1805	1480	1100	560

TABLE VII (Continued)							
D_{eff}^2 Corrected for 60° and Tracking cm^2							
λ, μ	Morning	Afternoon	Night		Hufnagel	Fried Night -	Day
0.6	96	24	400	144	96	52	10.3
1	322	81	1290	482	322	169	432
4	900	2290	3.6×10^4	144×10^2	900	49×10^2	1220
10	1.02×10^5	2.54×10^4	41×10^4	16×10^4	1.02×10^5	4.4×10^4	10^4
20	43.2×10^4	10.8×10^4	1.68×10^6	65.5×10^4	43.2×10^4	2.39×10^5	6.25×10^4

Tabulated is D_{eff}^2 . To obtain max signal power

$$P_{\text{max}} = \frac{\pi}{4} p D_{\text{eff}}^2$$

$$\text{Multiply by } \frac{\pi}{4} p = 0.786 p$$

To obtain power for aperture of D_{eff} , we multiply

$$\text{By } P_D = D_{\text{eff}} = \frac{1}{2.24} \quad P_{\text{max}} = \frac{1}{2.24} \quad \frac{\pi}{4} p D_{\text{eff}}^2$$

$$P_D = 0.351 p D_{\text{eff}}^2$$

$$p = \text{watts/cm}^2$$

D. HETERODYNE γ EFFICIENCY

A factor γ was defined by Gardner and used by Goldstein to denote the efficiency of a heterodyne detector; γ being the ratio of the effective signal power to the signal power available if no phase shifts were present. In the limit for large apertures R,

$$\gamma_{\text{Lim}} = \frac{2.48}{(ER)^2}$$

$$e = 2.91^{3/5} k^{6/5} \left(\int C_n^2 dx \right)^{3/5}$$

where

$$e^2 = 2.91^{6/5} k^{12/5} \left(\int C_n^2 dx \right)^{6/5}$$

The function $\gamma(R)$ is a complex one. We may use the above value only for large R ; in this case γ simply defines the signal power received by an aperture. Noting that $\gamma_{\text{Lim}} \sim \frac{1}{R^2}$, we see that since the power received with no fluctuations is proportional to R^2 , that γ_{Lim} defines the maximum signal power for any aperture.

Goldstein has performed the integration, and has plotted a normalized curve, $P_{\text{sig}}/P_{\text{max}}$, when P_{max} is the maximum power receivable, versus D/D_{eff} . He shows a 3.5 db loss at $D = D_{\text{eff}}$, which corresponds to the D^* of Fried for a phase shift of π . This is perhaps the most useful form of the plot, since it permits the calculation of the efficiency of utilization of the signal.

Our problem is thus reduced to calculating D_{eff} or the D^* of Fried, and from this we can obtain $P_{\text{sig}}/P_{\text{max}}$. Another technique would be to calculate P_{max} for a large aperture. This will simply be $\frac{\pi}{4} D_{\text{eff}}^2 p$, when p is the average signal density. The losses are then defined by the plot of P/P_{max} versus D/D_{eff} .

E. SCINTILLATION

Scintillation or fluctuations in the amplitude of the incoming signal is primarily caused by turbulence at higher levels. From Tatarski, assuming a 2/3 law, and $\sqrt{\lambda L} \gg \ell_0$, we may write

$$\sigma^2 = 2.24 k^{7/6} \int_0^L C_n^2 x^{5/6} dx$$

where, as before, the integration is along the line of sight. The integration weights values of C_n^2 at high altitudes, and it is here that we have the greatest uncertainty. Now σ^2 will be smoothed by the area of an aperture,

for $D \gg \sqrt{\lambda}L$ and σ small, the smoothing can be represented by a factor G ,

$$G \approx \left(\frac{D}{\sqrt{\lambda}L} \right)^{-7/3}$$

Thus, given the scintillation $\sigma^2 = \frac{(P-\bar{P})^2}{\bar{P}^2}$ for a given wavelength and aperture, it is possible to estimate σ for another wavelength and aperture. This eliminates the necessity of having to evaluate the integral.

Now we note that σ is a function of $\lambda^{-7/6}$, and that G is a function of $\lambda^{7/6}$, so that the averaged scintillation for a larger aperture is independent of the wavelength.

Thus, assuming typical values of σ^2 for various apertures, we may determine σ^2 for other apertures, independent of wavelength. Recognizing that values change considerably, let us assume $\sqrt{\lambda}L = 10\text{cm}$, and $\sigma^2 = 0.1$ in the winter and 0.05 in the summer. We then can calculate σ^2 for other apertures.

It should be noted that scintillation noise will appear in a heterodyne system as well as an amplitude system since it will appear as a fading of the signal; in this case the fluctuations will probably peak around 10 cps, and drop off extremely rapidly with frequency, because of the smoothing effect.

For large apertures σ^2 tends to go as $\sec^3 \theta$, where θ is the zenith distance. Thus for a zenith distance of 60° σ^2 will increase by a factor of 8. It should be noted that beyond 60° the \sec^3 relation fails, as it does also with small apertures.

DEFINITION OF SYMBOLS

$D_\phi(\rho)$	phase structure function, ρ is spacing
$\phi(\rho)$	phase as a function of position ρ
k	wave number
L	path length through medium
C_n	structure constant for index of refraction
ℓ_o	inner scale of turbulence
λ	wavelength
$b_A(\rho)$	correlation function
$\langle \rangle$	expectation value
D	aperture diameter
r_o	characteristic diameter, roughly coherence diameter
Δ	phase fluctuation
D_{eff}	effective diameter, roughly coherence diameter
L_o	outer scale of turbulence
p	signal power density (distinguished from previous ρ)
P	power (signal)
γ	heterodyne efficiency
σ	deviation of amplitude

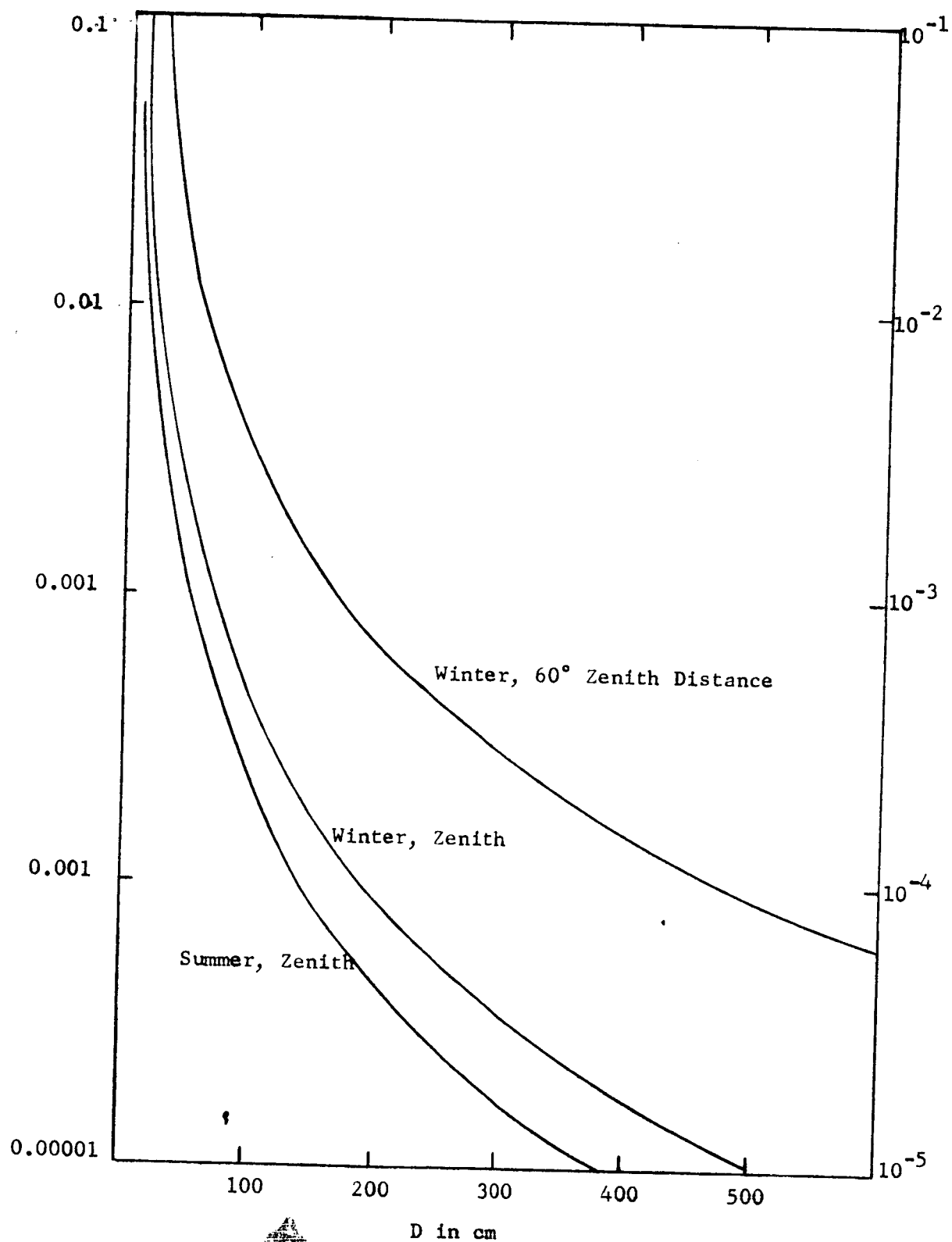


Figure 3 Scintillation vs Aperture

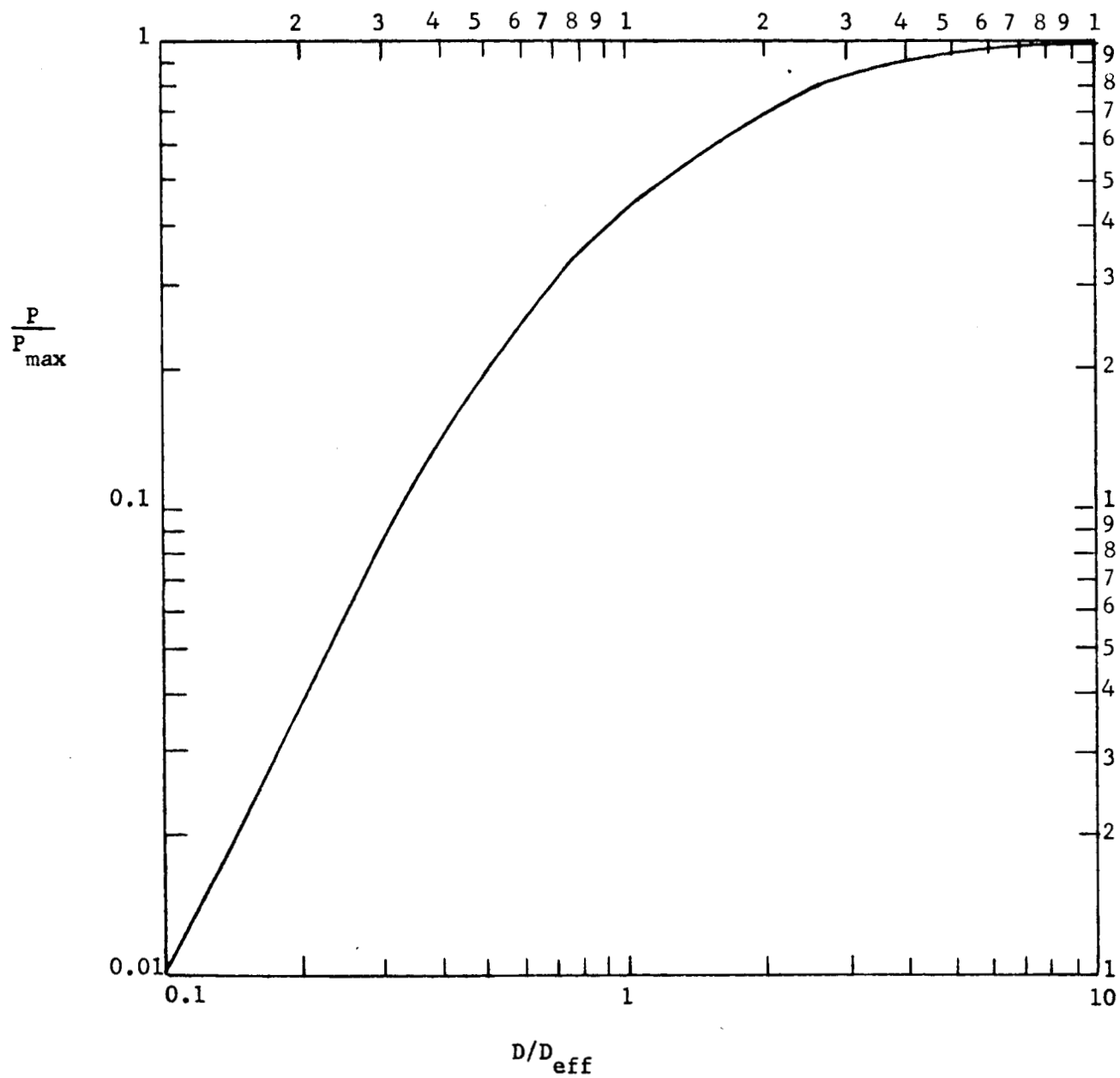


Figure 4. Detection Efficiency

F. SUMMARY

From the preceding discussion several points are apparent. First, at 10μ , it is possible to use coherent apertures of the order of 4 meters in size, day and night from a good location if image tracking is used. However, apertures drop down to the order of a meter in size if tracking is not used. Scintillation noise with these large apertures will be almost, if not, negligible. At 4μ the correlation distance drops to half a meter in the afternoon, but with tracking would be greater than two meters except for the worst part of the afternoon. Four microns with tracking corresponds roughly to ten microns without tracking. Wavelengths shorter than four microns do not appear to be usable with apertures of reasonable size. It should also be commented that in almost all cases it will be possible to track an object either in morning or evening twilight. It is hard to imagine a case in which it would be absolutely necessary to use the worst part of the afternoon. Thus the region with wavelengths longer than four microns is usable, especially if tracking is used. The advantages of tracking will decrease as the aperture approaches in size the outer scale of the turbulence, which will probably have an effective size of less than twenty meters. At twenty microns wavelength then, the gain due to tracking would begin to drop sharply.

From the standpoint of sky background and transmission, the regions just below 4μ and around 10μ appear the most favorable. The existence of a powerful laser near 10 microns seems to indicate that wavelength; although it would seem worthwhile to watch the situation between three and four microns closely, since at those wavelengths thermal radiation is much less of a problem than it is at 10 microns.

The treatment given here has been a static rather than a dynamic one, and it should be apparent that unless our aperture is much less than D_{eff} , there will be a fluctuating component to the signal as the actual correlation distance increases and decreases. A good analytical approach to this is not available, but from telescopic observations of seeing one might estimate that these fluctuations would tend to peak around ten cycles, and would give occasional bursts of high signal strength. At a first approximation, one might estimate that the effective aperture would vary from twice D_{eff} to half of D_{eff} , with the worst fluctuations existing at night and occurring at a fair amount lower than 10 cycles. This situation should be studied in more detail, since it is difficult to estimate with precision.

We must note that the use of an aperture larger than D_{eff} will not result in extra losses; it is just that it will not be effectively used. So from the standpoint of heterodyning, detection on oversize aperture does no harm. However, the total system noise will be a function of the total detector current, and a good portion of this will be set by the sky background. Thus, for the best signal-to-noise ratio, the aperture should be no larger than D_{eff} , since the extra aperture gathers no signal but does gather sky background.

Site location cannot be analyzed simply. The figures that we have given are those for a reasonably good site, but the parameters involved in defining a good site are not simple. Altitude is a factor, but local conditions are of such importance that one cannot consider altitude by itself. The location of good sites will probably depend on measurements on site and experience for a good number of years.

In summary, four and ten microns appear quite usable, especially if image motion compensation or tracking is used. Scintillation noise will be almost negligible. The aperture should be no larger than necessary to decrease sky background, but an oversize aperture has no effect on the signal.

The analysis should be carried further to see if it is possible to predict or analyze the dynamic behavior of the turbulence-induced phase shifts, which will have an effect on any signal-to-noise calculations, being a time varying fading on the signal. Neither this nor scintillation can properly be considered noise. It is possible that experimental determinations should be made. This could better be determined after further analysis.

SECTION IV

EFFECTS OF INCREASING ZENITH ANGLE ON OPTICAL SIGNALS

Reception of an electromagnetic signal through the atmosphere is directly affected by a number of factors which vary with zenith angle. These phenomena include sky background, atmospheric absorption, wavefront coherence diameter, probability of cloud cover, and scintillation effects.

An obvious result of increasing zenith angles is the corresponding increase in the equivalent number of air masses along the line of sight. The number of air masses is nearly equal to the secant of the zenith angle (2.0 air masses at 60° zenith angle, 2.9 at 70°, 5.6 at 80°) until close to the horizon, where the number of air masses is between 28 and 30.

Sky background results from scattering and from thermal emission of the atmosphere, the latter effect depending upon the emissivity and temperature of the air along the line of sight. For wavelengths shorter than three microns, scattering predominates and is, of course, a function of wavelength and of the sun's position. Zenith sky spectral radiance at 0.6 microns, for example, is on the order of 4×10^{-4} watts - cm⁻² - strd⁻¹ - micron⁻¹ in the daytime, dropping as much as two orders of magnitude at twilight and six orders of magnitude in the middle of the night. At a wavelength of 1.0 micron, the zenith sky spectral radiance is roughly one-fourth that at 0.6 microns, but does not drop much past twilight values due to OH molecular radiation from the upper atmosphere. Between 2.5 and 4 microns, the zenith sky background is very slight, much less than 10^{-6} watts - cm⁻² - strd⁻¹ - micron⁻¹. This region of the spectrum is a crossover point where the wavelength is too long for appreciable scattering but too short for any substantial thermal emission. At wavelengths above four microns,

thermal emission predominates and increases rapidly to about 10^{-4} watts - cm^{-2} - strd^{-1} - micron^{-1} .

For purposes of rough approximation, the sky background may be considered generally proportional to secant of the zenith angle. i.e. to the number of air masses along the line of sight. It must be emphasized, however, that no simple theory applies and that accurate prediction of background conditions at any zenith angle is a formidable task.

Atmospheric absorption is similarly complex. particularly in the infrared where absorption depends on the precise wavelength involved and on the absorption bands of the various gaseous components of the atmosphere.

In the visible wavelengths, atmospheric attenuation is equivalent to 0.21 magnitude per air mass for visual magnitudes or 0.44 magnitude per air mass for photographic magnitudes. This amounts to a 1.7 db loss per air mass in the blue, 0.8 db loss per air mass in the visual region, and on the order of 0.4 db loss per air mass in the photographic infrared. Applying the latter number to a 0.6 micron laser, for example, yields expected losses of 0.8 db, 1.2 db, and 2.2 db at zenith angles of 60, 70, and 80 degrees, respectively.

In the 1.0 micron region, scattering and absorption by water vapor predominate. For 1.0 precipitable centimeter (pr.cm) of H_2O , the transmission (due to water vapor) varies from 99.5 percent at 1.03 microns to 4 percent at 1.35 microns, with a secondary peak of 96 percent at 1.2 microns.

In the 4 micron region, 0.1 pr. cm H_2O yields transmissions in most instances of 95 percent or more from 3.5 to 4.8 microns, peaking at 99.6 percent at 4.1 microns. However, strong CO_2 bands with transmission of virtually zero exist below 3.0 microns and above 3.9 microns.

From 9.8 to 10.1μ , CO_2 is transparent, with bands on each side. Although these bands are not extremely strong (for zenith distance $<80^\circ$ they have transmission of 90 percent), the actual transmission would depend on the precise wavelength. H_2O transmission for 1.0 pr. cm, would be near 97 percent for 10μ . Ozone also has a strong effect here.

At 20 microns, 0.1 pr. cm of H_2O would drop transmission below 80 percent, and one is just beyond the edge of strong CO_2 bands.

It is apparent that precise atmospheric losses depend critically on wavelength and band structure. In addition, as one approaches the horizon, haze scattering becomes important. This factor depends strongly on site location.

Another factor of importance in systems employing coherent detection is maximum coherence diameter, which varies as $\theta^{-3/5}$, where θ is the zenith angle. If the limiting factor is coherence diameter, the received power at zenith angles of 60, 70, and 80 degrees is, respectively, 0.44, 0.29, and 0.12 of the zenith received power.

Another difficulty, which may occur at any of the wavelengths under consideration, is the existence of clouds. As the line of sight approaches the horizon the probability of cloud obscuration increases rapidly. One might expect that the probability of having a cloud in the line of sight increases with the path length through the level at which the clouds occur, which leads to an estimate of the increase in the probability of the order of the secant of the zenith distance.

Scintillation is also a function of zenith distance ($\sigma^2 \sim \sec^3 \theta$) and would degrade signal quality near the horizon. The relation shown breaks down very close to the horizon and scintillation tends to saturate. Variations in transparency, which occur with low frequencies and resemble low frequency scintillation (cycles per minute) will also increase with zenith distance, making the situation even worse.

In summary, it is evident that large zenith angles will result in serious degradation of the received signal. If signal attenuation is estimated to vary as $\sec \theta$ and the power receivable at the limiting coherence diameter varies with $\sec^{-6/5} \theta$, the overall losses will vary as $\sec^{11/5} \theta$, or somewhat faster than $\sec^2 \theta$. At zenith angles of 60, 70, and 80 degrees, losses estimated on this basis increase over zenith conditions by factors of 4.6, 9.5, and 44, respectively. While the approximations are admittedly somewhat crude, it is plain that zenith angles much in excess of 60 or (at most) 70 degrees will result in losses of sufficient magnitude to make this portion of the sky of questionable usefulness for optical communication.

SECTION V

TELESCOPE CONFIGURATIONS FOR INCOHERENT DETECTION

A. GENERAL

The following paragraphs consider some of the important parameters governing the design of a large aperture telescope of the energy-collecting or "photon bucket" category. A number of alternative configurations are considered, and an attempt is made to delineate the advantages and the shortcomings of each. Emphasis has been placed on establishing the inherent feasibility of each approach rather than on investigating the mechanical details involved.

While the discussion is deliberately couched in general terms, insofar as practical, an aperture diameter of 10 meters is employed wherever consideration of specific dimensions is considered useful.

It will quickly become apparent that two of the principal factors influencing design of the instrument are desired sky coverage and required area of the primary mirror. A few comments on these topics precedes discussion of particular configurations.

1. Sky Coverage Requirements

Selection of the optimum configuration for the proposed giant aperture telescope is necessarily influenced by the regions of the sky towards which the telescope must be capable of pointing. A number of possible sky coverage requirements are possible, and the relative advantages of each must be weighed against the technical and economic feasibility of implementing the instrument required.

a. Hemispheric Coverage

The upper bound on sky coverage capability is, of course, the

ability to look at an object anywhere in the celestial hemisphere, i.e. any object above the horizon. Coverage of the entire celestial hemisphere requires 360 degrees of azimuth angle capability and 90 degrees of elevation angle capability, and provides coverage of a solid angle subtending 2π steradians.

Obviously, this kind of coverage would represent the ultimate in system capability and flexibility. As will become apparent, however, implementation of such capability in a giant aperture telescope can involve problems of considerable magnitude.

b. Zodiac Coverage

If the proposed telescope is to be used to communicate with vehicles traveling to the planets or otherwise in the general vicinity of the ecliptic plane, sky coverage requirements may be correspondingly reduced.

The nature of the coverage required may be determined by inspection of Figure 5, which diagrams the celestial sphere as viewed by an observer at point "O" at latitude "L" in the northern hemisphere. The north celestial pole appears at an angle "L" above the northern horizon. The celestial equator is co-planar with the earth's equator, and the ecliptic plane intersects the equatorial plane along a line extending from the observer towards the vernal equinox, γ . As shown, the angle between the ecliptic and equatorial planes is $23^{\circ}27'$. The entire celestial sphere rotates about the polar axis in an east-to-west direction with respect to the observer.

It is apparent that, as the celestial sphere rotates, the ecliptic plane sweeps out a band or zone $46^{\circ}54'$ wide centered about the celestial equator. Consequently, if the observer wishes the capability of tracking an object anywhere in the ecliptic plane at any time that said object is above the horizon, he must be equipped to direct his instrument to any spot in the zone described.

The planets are all confined to a narrow band of sky, the zodiac, centered around the ecliptic. Hence, by reasoning similar to the above, the capability of looking at a planet at any time when it is above the horizon requires coverage of a zone of the celestial sphere centered about the

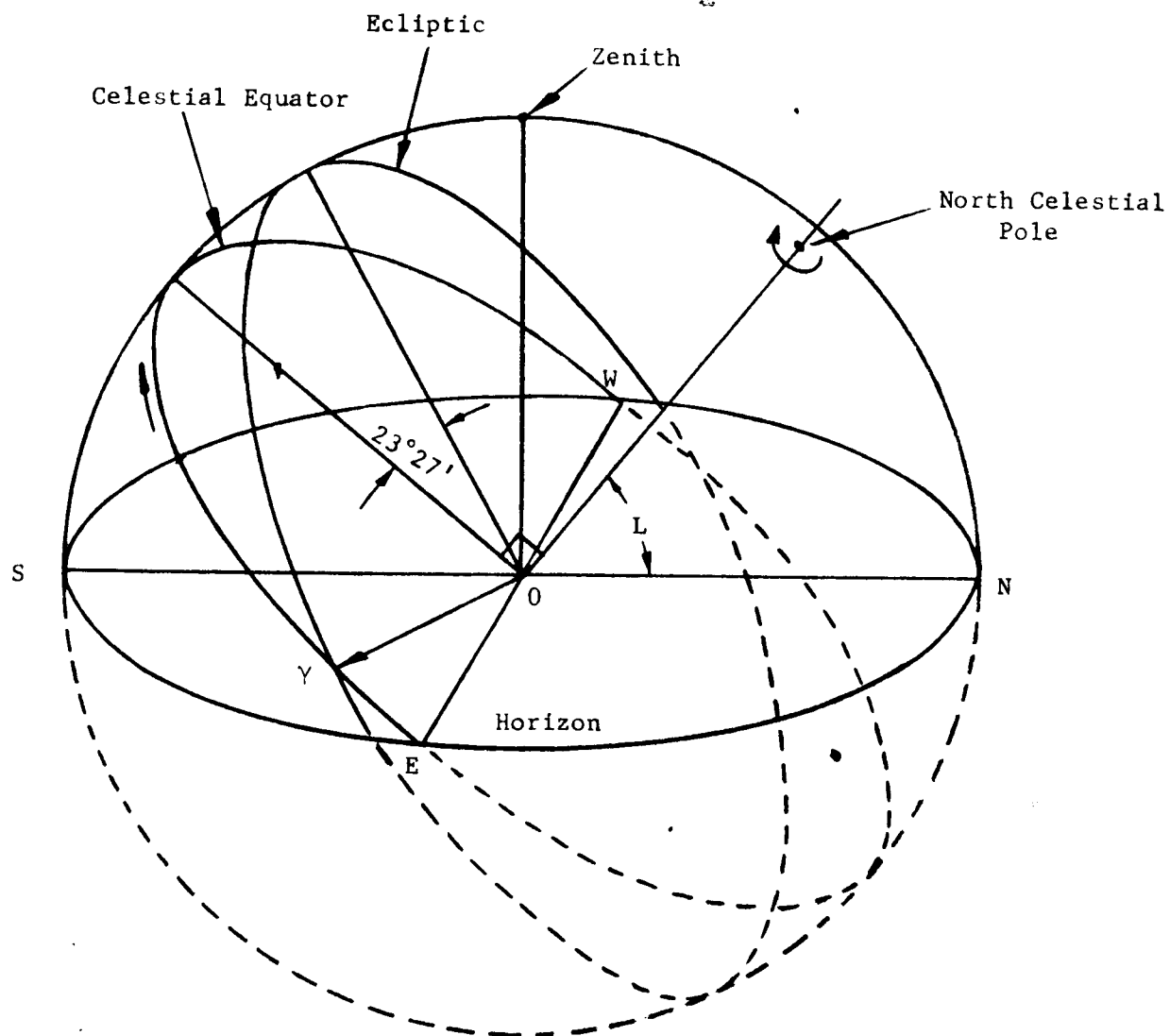


Figure 5. The Celestial Sphere as Viewed by an Observer at Latitude L in the Northern Hemisphere

celestial equator and with an angular width of $2(23^{\circ}27' + i_p)$, where i_p is the maximum angular departure of the planet from the ecliptic, as seen from Earth. The illustration (Figure 6) shows this zone for an observer at a typical latitude L . Figure 7 shows the same area of the sky in a somewhat simplified diagram that also indicates some of the limiting elevation and azimuth angles. Inspection of this figure reveals that zenith pointing is required for observing latitudes $\leq (23^{\circ}27' + i_p)$. Similarly, the amount of horizon coverage required increases from $4(23^{\circ}27' + i_p)$ at 0° latitude to 360° at latitudes $\geq (66^{\circ}33' - i_p)$.

A survey of orbital parameters for all the planets reveals that the maximum conceivable value of i_p would occur in the case of an inferior conjunction with Venus at a time when that planet is at its maximum distance from the ecliptic. Figure 8 illustrates the geometry of this situation and shows the worst-case value of i_p to be $8^{\circ}46'$.

Substituting $i=8^{\circ}46'$ into the expressions cited above, it is found that zenith pointing is required at latitude $\leq 32^{\circ}13'$ and that the angular extent of horizon coverage required increases from $128^{\circ}52'$ at equatorial observing sites to 360° at latitudes $\geq 57^{\circ}47'$. Similarly, it is found that the solid angle subtended by the sky coverage described is 3.35 steradians or 53.3% of the celestial hemisphere.

It should be noted that the situation described by Figure 8 is a relatively infrequent occurrence and that some reduction in i_p capability might be contemplated if occasional lapses of coverage were acceptable. (Inferior conjunctions of Venus occur at approximately 1.6 year intervals, with each displaced by about 218° from the preceding one.) However, the acceptable reduction for a system with a lifetime of many years would be quite small and would not significantly alter conclusions based on consideration of the worst-case condition.

2. Primary Mirror Area Requirements

A fundamental factor differentiating the various telescope concepts is the area of primary mirror required. To a considerable degree, the question

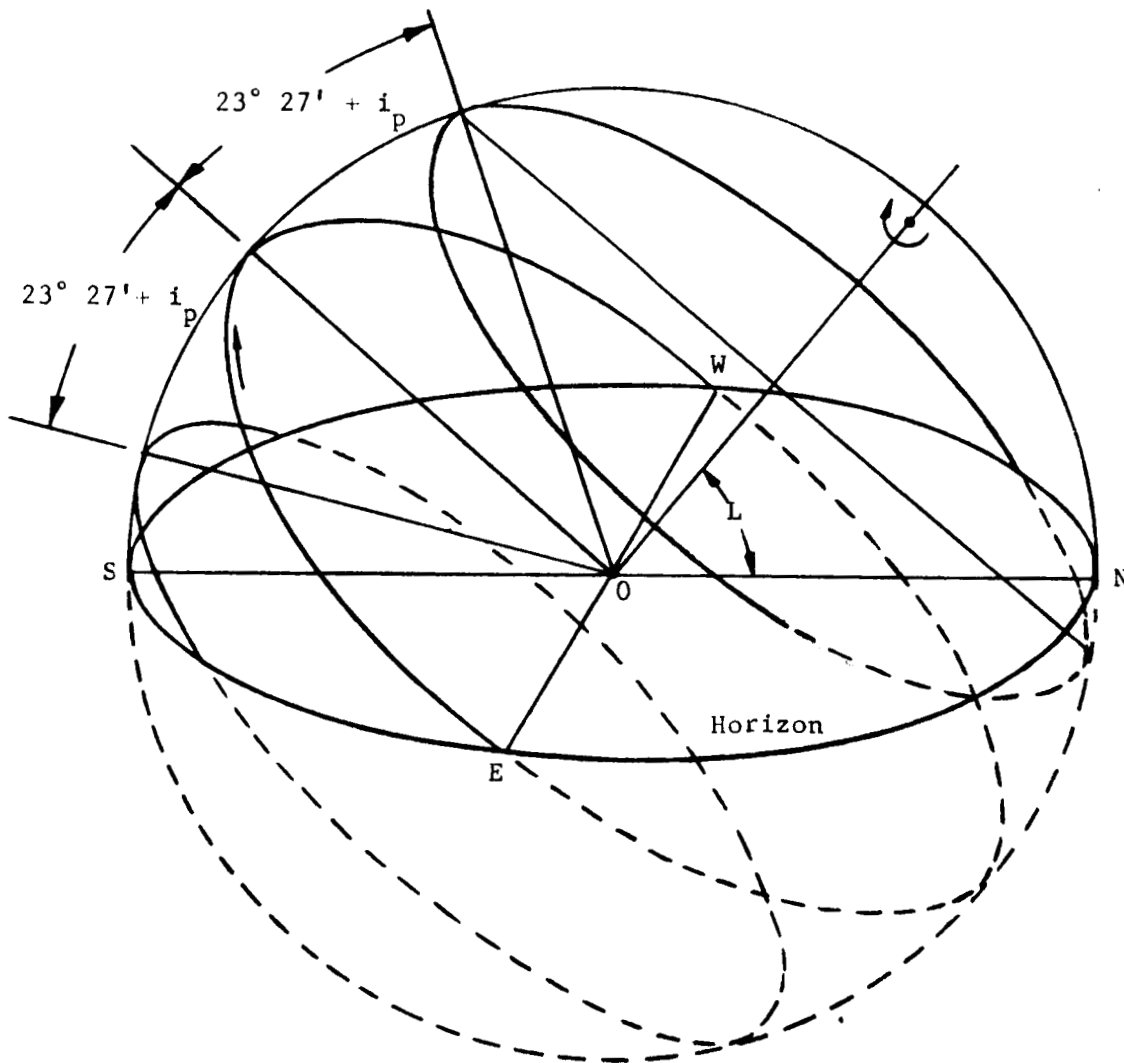
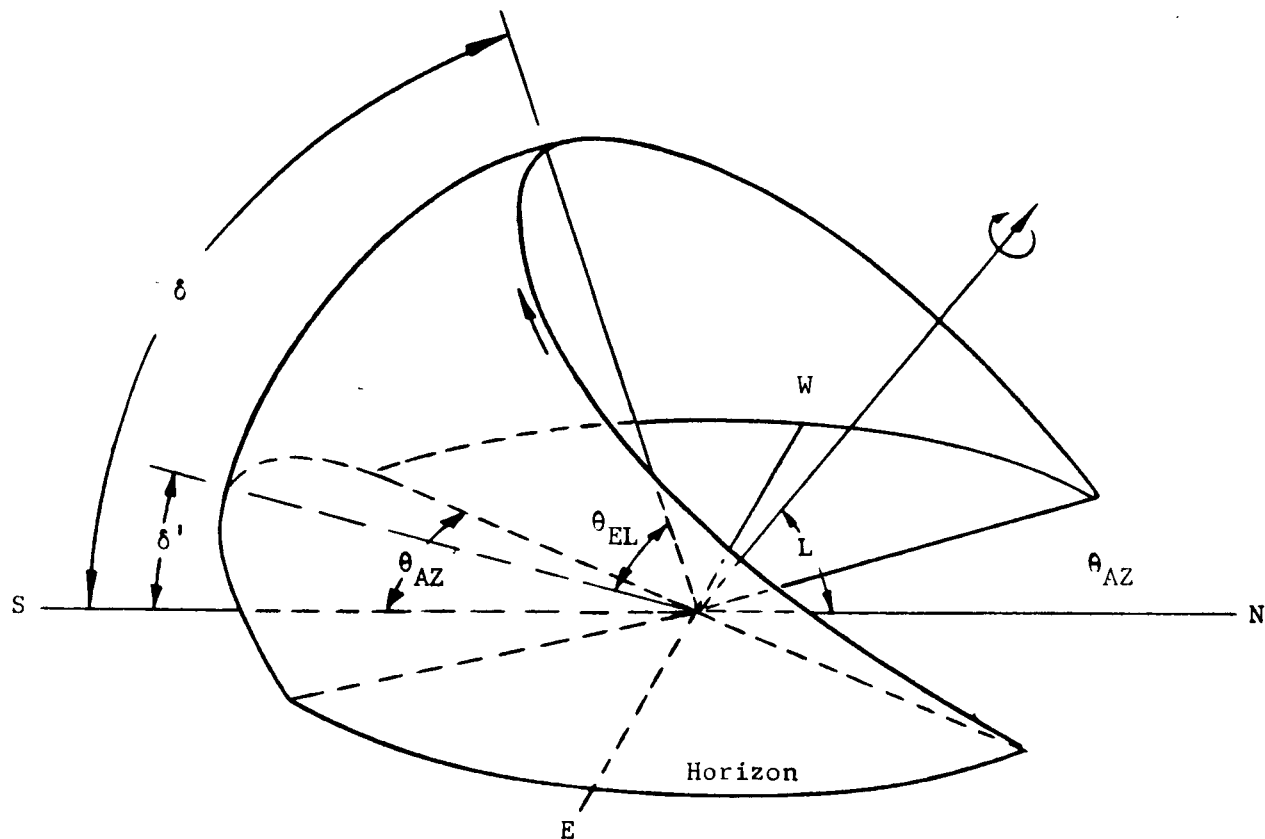


Figure 6. Sky Coverage Required to Assure Capability of Tracking an Object i_p out of Ecliptic Plane



$$\begin{aligned}\delta &= 90^\circ - L + 23^\circ 27' + i_p \\ \delta' &= 90^\circ - L - 23^\circ 27' - i_p \\ \theta_{EL} &= 46^\circ 54' + 2 i_p \\ \theta_{AZ} &= \cos^{-1} \left[\frac{\sin(23^\circ 27' + i_p)}{\cos L} \right]\end{aligned}$$

Figure 7. Limiting Angles Associated with Sky Coverage Described by Figure 6.

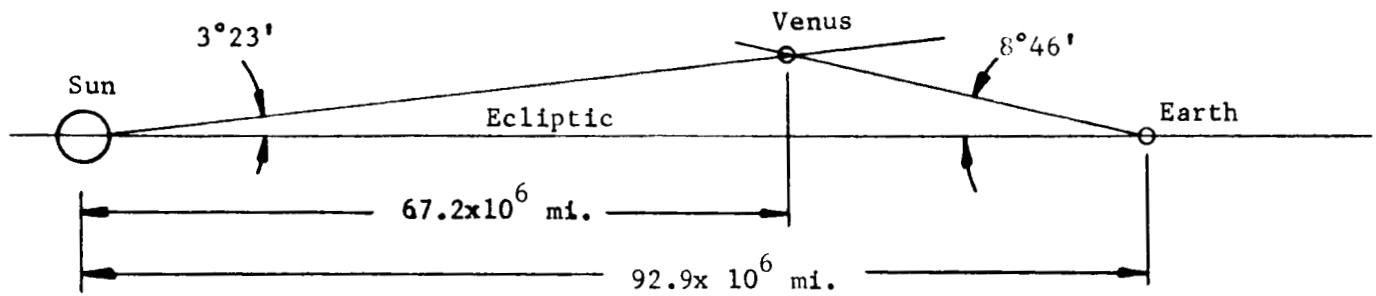


Figure 8. Worst Case Angular Departure of a Planet from the Ecliptic, as Seen from Earth

resolves itself to the economic trade-offs between increased mirror area and increased structural and mechanical complexity.

For aperture diameters on the order of 10 meters, it seems inescapable that the only practical approach is the use of a segmented mirror. It likewise seems apparent that the most promising method of economically fabricating a large number of similar segments, with the required degree of radius matching, is by replication. This is an area in which considerable groundwork has been established, but which would require additional development in terms of the particular requirements of this study. Typical of the questions requiring investigation are the optimum size and shape of the segments.

The mirror area requirements of a number of possible configurations are indicated in the following paragraphs.

B. FIXED SPHERICAL REFLECTOR

A major problem area confronting the designer of large-aperture ground-based telescopes is the sensitivity of the primary mirror and its supporting and locating structure to the influence of gravity. This difficulty is compounded in conventional instruments by the necessity for operation in various and continually changing orientations with respect to the gravity vector.

The usual solution to this problem is an elaborate and carefully executed system of counterweights designed to balance out gravitational forces in an approximately uniform manner regardless of orientation. For single piece reflectors, this approach proves to be effective and practical.

Contemplation of apertures so large that the primary mirror must consist of a number of segments poses new aspects of the problem. While each segment might be successfully counterweighted to minimize distortions of its surface, maintenance of accurate alignment of those segments to each other requires one or more of the following alternatives:

- (1) Continuous mechanical realignment of each segment to compensate for varying gravity deflections of the support structure.
- (2) Provision of a second level of counterweights to compensate for gravity deflections of the structure, which supports and positions the counterweighted segments.
- (3) Provision of entirely separate load-bearing and positioning structures, with the latter called upon to carry no loads (even its weight would have to be transferred to the load-bearing structure).

All of these possibilities are sufficiently unattractive to encourage the search for approaches other than that typical of conventional astronomical telescopes.

One interesting concept is the complete avoidance of varying gravity deflection problems in the primary mirror by fixing that element of the system with respect to the gravity vector. Such a system might consist of a fixed spherical primary mirror in combination with a relatively small and manageable secondary optics package that, for tracking, rotates about the center of curvature of the primary. Figure 9 diagrams such a configuration.

The major advantage of this approach is the relative simplicity of the primary mirror support problem. The various segments would be rigidly and securely positioned on a massive and rigid foundation, with no concern whatever for static deflections except for possible long term thermal and soil-stability effects.

It is immediately apparent, however, that the principal penalty for avoiding the varying gravity vector in this manner is a significant increase in the reflector area required. The portion of the mirror employed at any one time is about equal in area to the aperture required, while the total

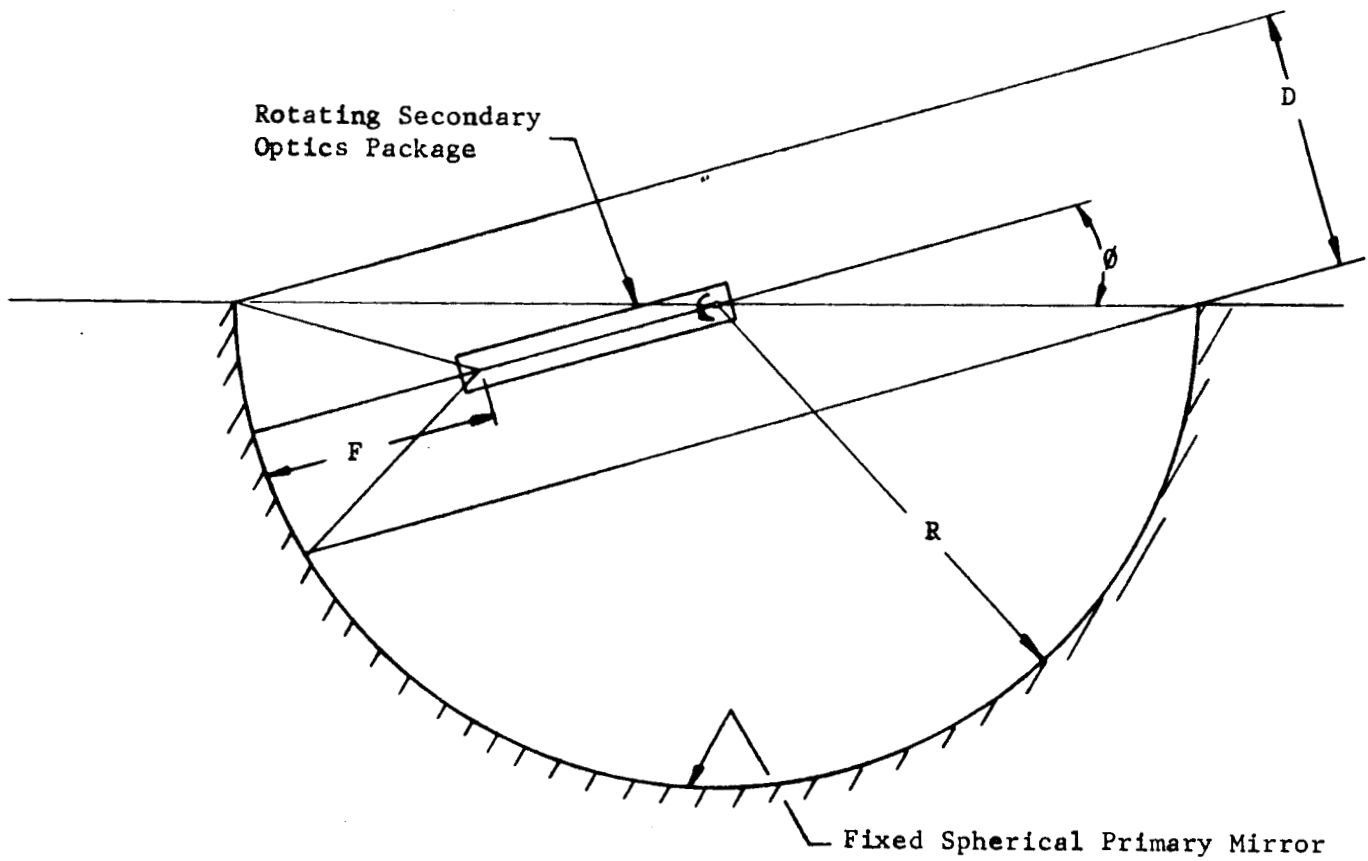


Figure 9. Telescope with Fixed Spherical Primary Mirror

mirror area needed is also a function of sky coverage desired.

If coverage of the entire celestial hemisphere is required (ignoring for the moment the problem of self-vignetting at low elevation angles), the primary mirror must itself be a complete hemisphere. It is apparent from Figure 9 that the ratio of mirror area to aperture area is simply

$$\frac{A_{\text{mirror}}}{A_{\text{aperture}}} = \frac{2\pi R^2}{\pi D^2/4} = 8 \left(\frac{R}{D} \right)^2 = 32 \left(\frac{F}{D} \right)^2 = 32 \left(f/\text{no.} \right)^2$$

This relationship is plotted in Figure 10 and illustrates the urgency of employing the fastest possible primary mirror to keep the required primary mirror size within manageable bounds.

If zodiac coverage rather than hemisphere coverage is desired, the required mirror area decreases as a function of the decreased sky coverage. The mirror configuration required at a northern latitude L is depicted in Figure 11, and is merely a projection of the sky illustrated by Figure 7 with two added strips equal in width to half the aperture diameter. The surface area of such a mirror, expressed as a multiple of the aperture area, turns out to be

$$\frac{A_{\text{mirror}}}{A_{\text{aperture}}} = 32 \left(f/\text{no.} \right)^2 \sin \left[23^\circ 27' + i_p + \sin^{-1} \left(\frac{1}{4 \times f/\text{no.}} \right) \right]$$

regardless of latitude. This relation also is plotted in Figure 10 for the previously discussed value of $i_p = 8^\circ 46'$. Comparison of the two solid curves in Figure 10 demonstrates that the percentage reduction in glass area requirements, which results from decreasing coverage from hemisphere to zodiac, increases with $f/\text{no.}$ Reductions of 27 percent at $f/1.0$ and 42 percent at $f/4.0$ are representative. (The dashed curve in this figure refers to an alternative concept, to be discussed in a following section.)

A second shortcoming of the fixed spherical reflector, alluded to above and evident from Figure 9, is loss of horizon coverage due to self-vignetting of the mirror at low elevation angles. For either the hemispheric

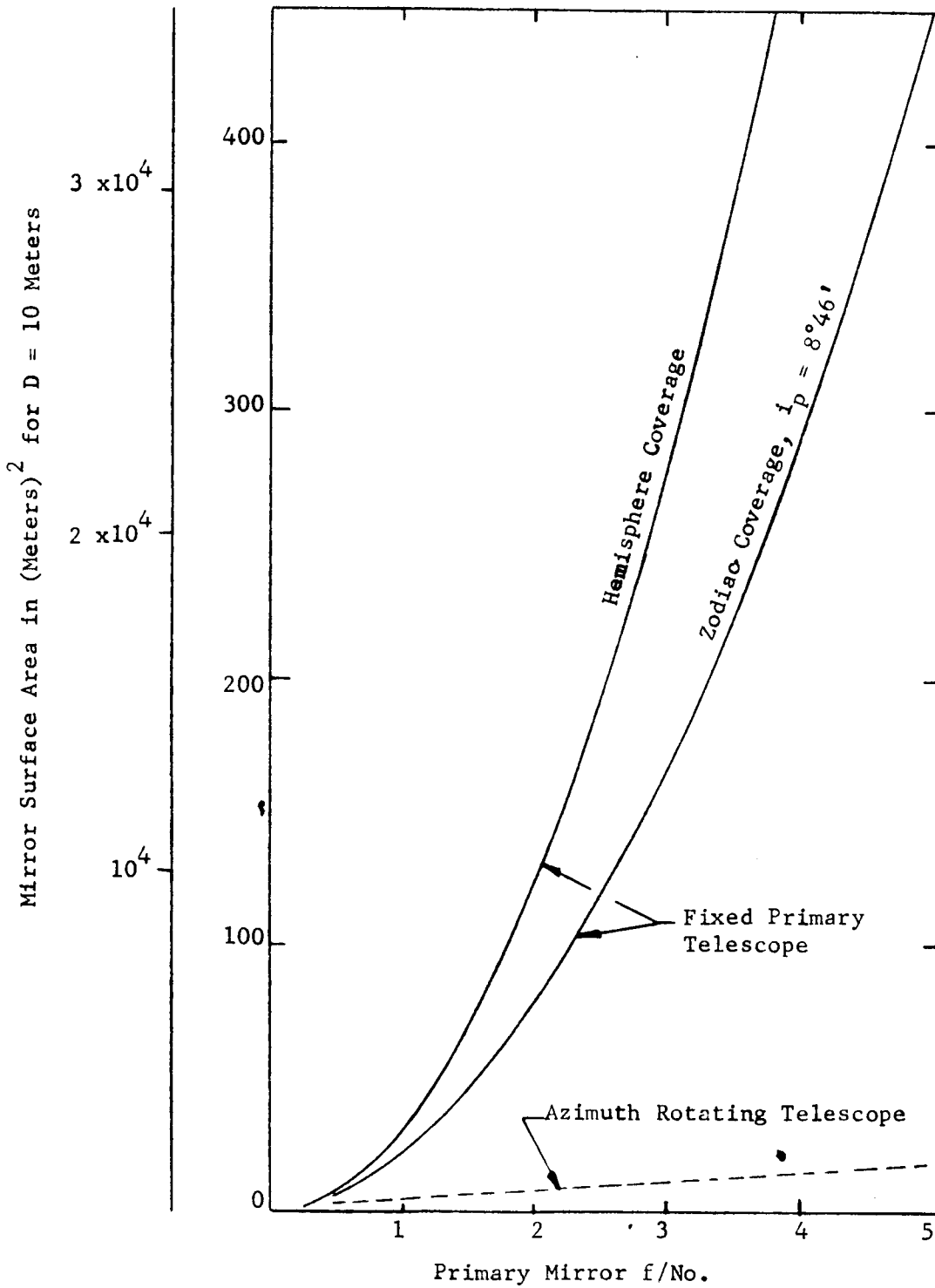


Figure 10. Primary Mirror Surface Area vs f/No.

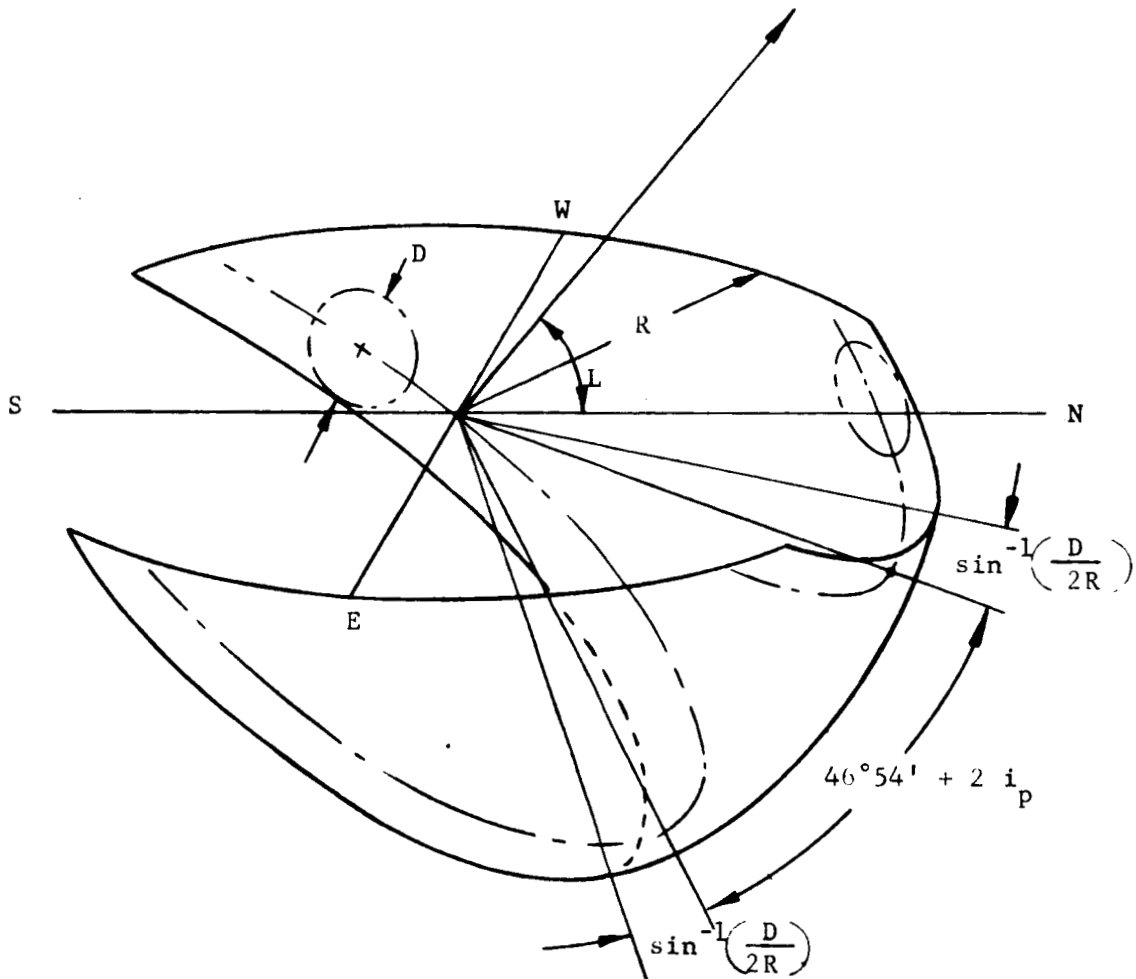


Figure 11. Mirror Configuration For Zodiac Coverage

or the zodiac coverage, the minimum unvignetted elevation angle is

$$\phi = \sin^{-1} \left(\frac{D}{2R} \right) = \sin^{-1} \left(\frac{0.25}{f/no} \right)$$

If some degree of vignetting is acceptable, lower values of elevation angle may be employed. Figure 12 shows, as a function of primary mirror f/no., the minimum elevation angle for an unvignetted aperture and the elevation angles corresponding to vignetting of one-third and two-thirds of the aperture area.

It should be noted that the obvious advantages of the slower primary mirrors in terms of low elevation angle coverage are in direct conflict with the previously demonstrated necessity of fast mirrors if the mirror surface area requirements are to be kept within attainable limits.

Several possibilities exist for circumventing the loss of horizon coverage by a fixed dish.

If, for example, one begins with a fixed hemispherical reflector and a desire to alter it in a manner permitting horizon coverage, one might institute the following changes, as illustrated by Figure 13.

- (1) To eliminate self-vignetting of the mirror when looking at the western horizon, remove a strip of mirror equal in width to half the aperture diameter from the western half of the hemisphere's periphery.
- (2) To intercept the light, which otherwise would not be collected when looking at the western horizon, add an identical strip of mirror to the eastern half of the hemisphere's periphery.

At this point, the system is capable of unvignetted coverage of the western horizon, but vignetting begins at an angle of $2 \sin^{-1} \left(\frac{D}{2R} \right)$ above the eastern horizon.

- (3) Construct, at an adjacent but separate location, a supplementary zonal mirror equal in width (approximately) to 2D

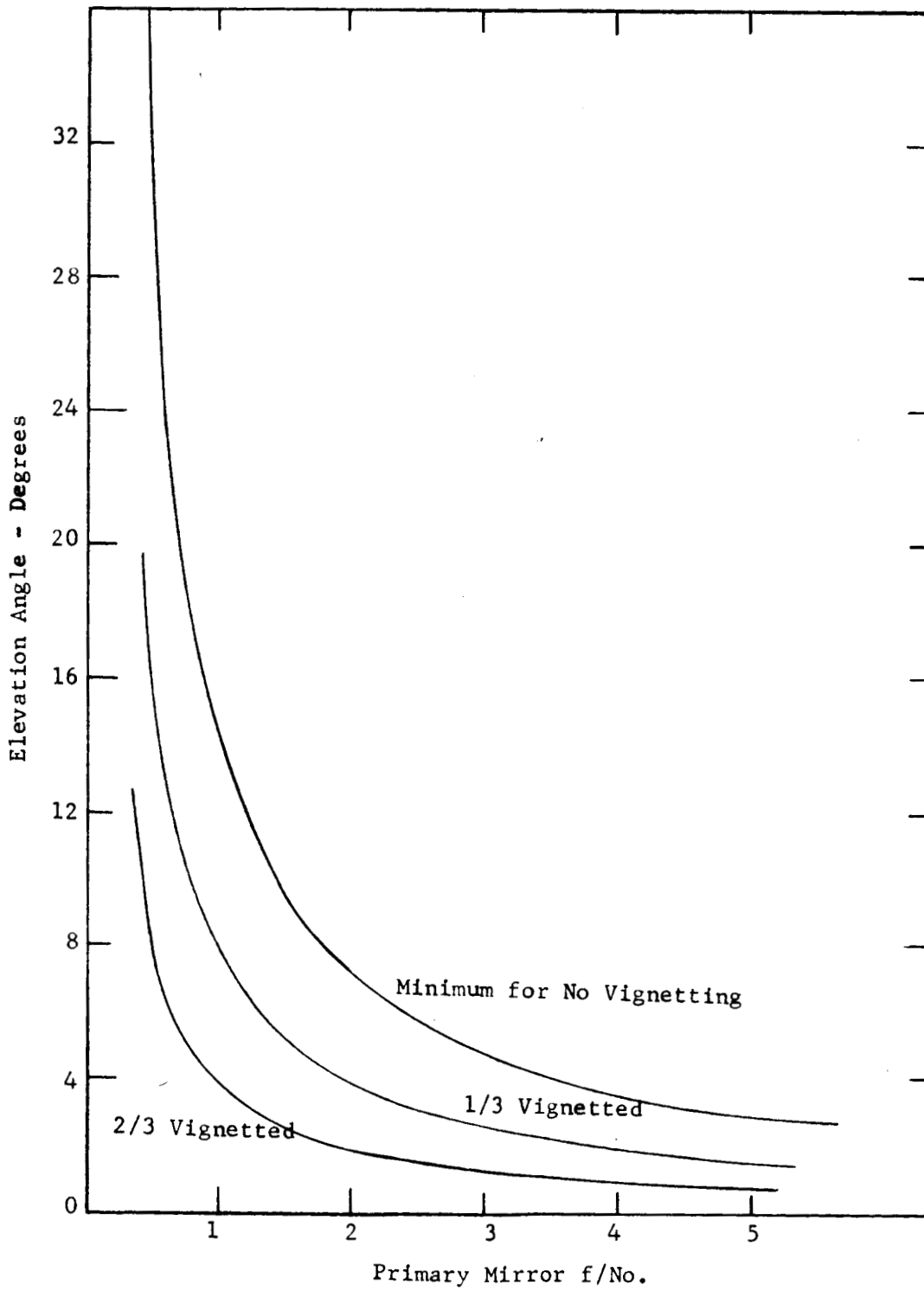


Figure 12. Minimum Elevation Angle vs Primary Mirror f/No.
For Various Degrees of Vignetting

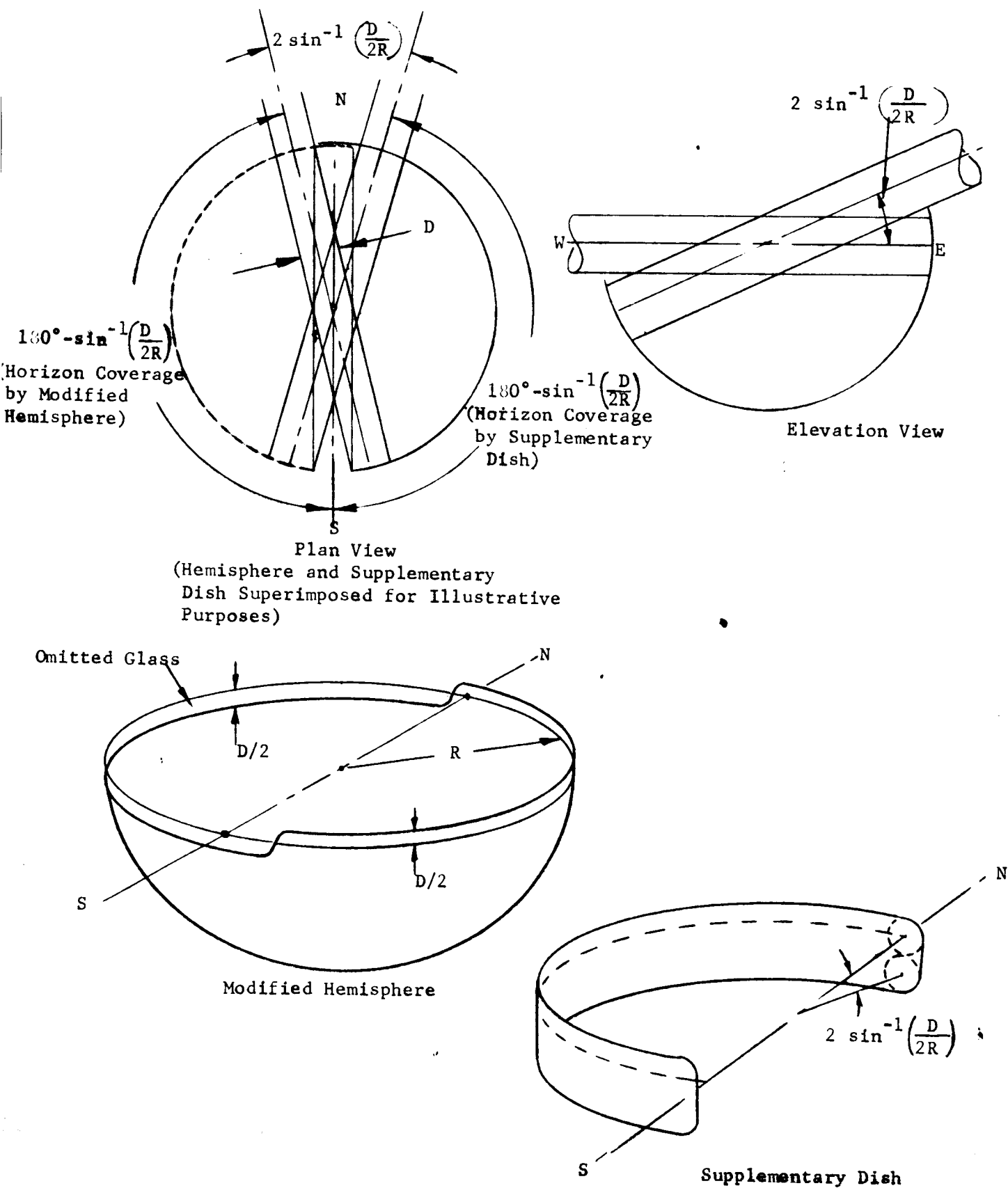


Figure 13. Glass Requirements for Full Horizon Coverage

to provide unvignetted coverage of the eastern horizon.

The resulting system is capable of full coverage of the celestial hemisphere with the exception of a "blind spot" subtending $2 \sin^{-1} \left(\frac{D}{2R} \right)$ of the northern horizon for the case illustrated. It is evident, however, that a penalty has been paid in terms of an increase in mirror surface area equal to the area of the supplementary dish. Of even more serious consequence is the requirement for a complete duplication of the secondary optics and detector systems in conjunction with the supplementary mirror. It is thus plain that the addition of horizon coverage to the fixed primary mirror system would involve substantial increases in the cost and technical complexity of the installation.

It is true that there are a variety of ways in which the total mirror area might be divided between the two fixed mirrors, but the above comments would remain applicable in any event. Similarly, application of the above approach to the case where only zodiac coverage is desired, again leads to the inescapable requirement for dual optical systems and somewhat greater total mirror area than if horizon coverage were deleted.

Table VIII summarizes representative computations of mirror area requirements for hemispheric and zodiac coverage with and without horizon capabilities.

•

An interesting possibility of obtaining horizon coverage with less total area and without dual systems is available if a partial departure from the completely fixed dish is allowed. The proposed approach is diagrammed in Figure 14, and consists of a fixed dish (less than a full hemisphere) in combination with a movable extension mirror that may be positioned anywhere around the periphery of the fixed dish to provide horizon coverage. Such a system would provide true hemispheric sky coverage with no "blind spots," would utilize a single secondary optics and tracking system, and would actually require less total glass area than a simple hemispheric reflector. The disadvantage, of course, is the requirement for moving and accurately aligning the movable horizon scanner portion of the mirror. The fact that this movable portion rotates around a vertical axis does not introduce any problem of varying

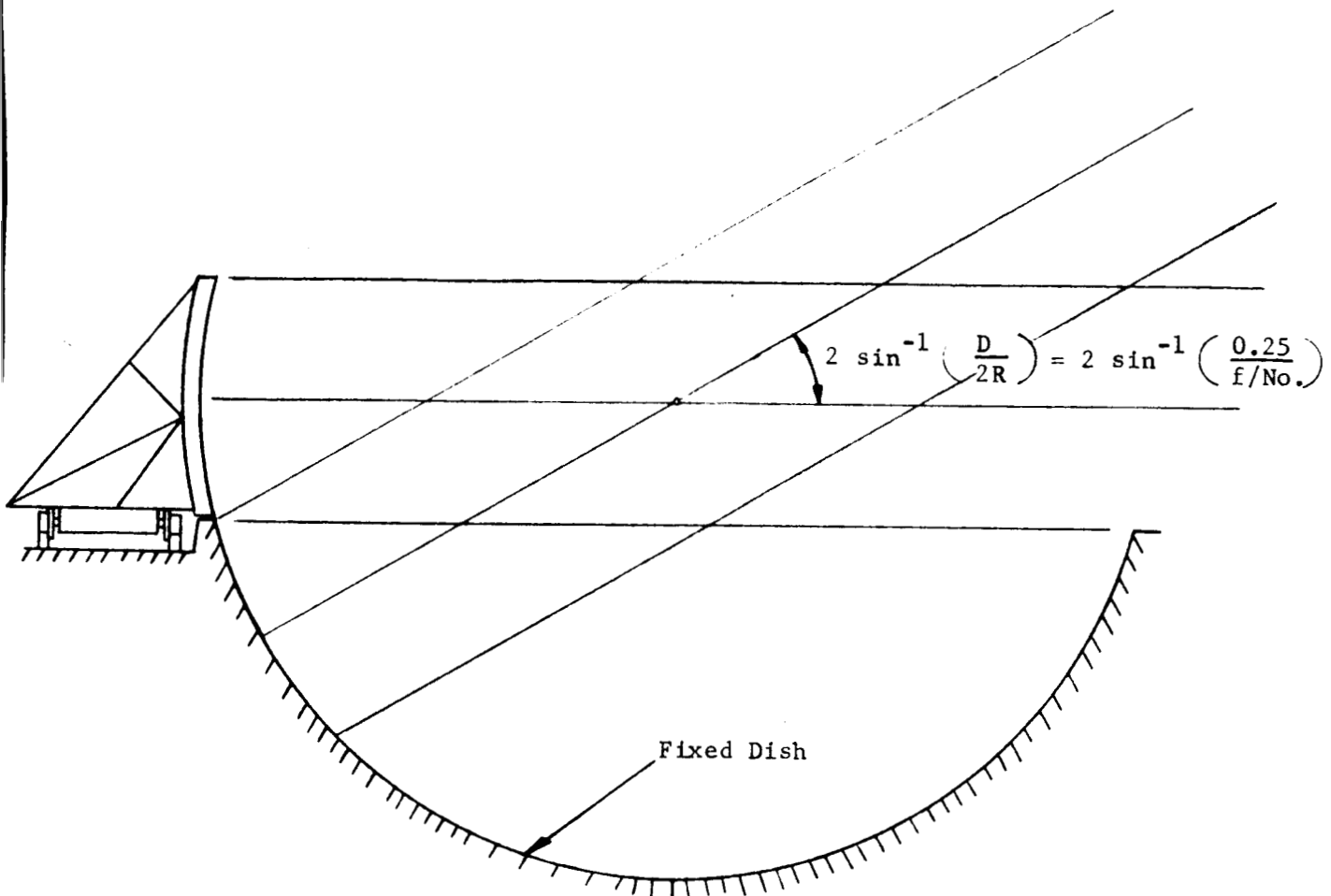
TABLE VIII

MIRROR AREA REQUIREMENTS

	HEMISPHERE COVERAGE			ZODIAC COVERAGE			
	Excluding Horizon (Single Dish)	Including Horizon (Double Dish)	Excluding Horizon (Single Dish)		Including Horizon (Double Dish)		
					L=0°	L=20°	L=40° L= 60-90°
<u>Glass Area</u> Aperture Area f/0.5 f/1.0 f/2.0 f/4.0	8.0 32.0 128.0 512.0	13.9 46.7 159.5 574.7	7.1 23.3 81.3 299.0		12.9 30.6 91.0 315.0	13.1 30.9 91.9 315.0	13.5 32.0 93.6 318.0 15.6 35.6 102.0 335.0
<u>Glass Area</u> (Meter ²) For D=10 Meters f/0.5 f/1.0 f/2.0 f/4.0	628 2513 10053 40212	1092 3668 12527 45137	558 1830 6385 23483		1013 2403 7147 24662	1029 2427 7218 24740	1060 2513 7351 24975 1225 2796 8011 26311
<u>Minimum</u> Unvignetted Elevation Angle f/0.5 f/1.0 f/2.0 f/4.0	30° 14.5° 7.2° 3.6°	0° 0° 0° 0°	30° 14.5° 7.2° 3.6°		0° 0° 0° 0°	0° 0° 0° 0°	0° 0° 0° 0°

*One "Blind Spot Will Exist on the Horizon

4047 M² = One Acre



f/No	$2 \sin^{-1} \left(\frac{0.25}{f/No} \right)$	$\frac{A_{\text{Fixed Dish}}}{A_{\text{Aperture}}}$
0.5	60°	4
1.0	29°	24
2.0	14°	112
4.0	7°	480

Figure 14. Fixed Dish + Movable Horizon Scanner

gravity deflections. In addition, the alignment problem would not represent a substantial increase in technical difficulty since even the fixed dish would almost certainly require means for rapid and routine alignment of its various segments.

1. Tentative Optical Design

In order to establish the feasibility, in terms of optical design, of the systems described in foregoing paragraphs, tentative computations on one possible configuration have been performed. The inputs to the selection of this configuration included the following.

- (1) The primary mirror must be a true sphere, with a clear aperture of 10 meters \approx 400 inches.
- (2) The operating f/no. of the primary mirror should be as low as practical in order to minimize the total area of the fixed mirror.
- (3) To enhance the flexibility and utility of the instrument, an all-reflective system is desirable.
- (4) The instrument should have a nominal field of view of 20 seconds of arc (per acquisition requirements determined in OTS studies, but subject to additional evaluation), and resolution capability consistent with the small field of view, i.e. a few seconds of arc.
- (5) The optical system should include collimated or high f/no. beam of reasonably small diameter to permit insertion of required pre-detection optical filters.
- (6) The secondary optics should be compact, to minimize obscuration of the primary, and should be amenable to straight-forward mounting and positioning techniques in the rotating support structure.

The configuration selected to meet these specifications is shown in Figure 15 and consists of the 400-inch diameter spherical primary mirror, a 48-inch diameter concave aspheric secondary mirror, and a 9-inch diameter convex aspheric tertiary mirror. The primary mirror is $f/0.95$, and the system is $f/30$, giving an EFL of 300 meters \approx 1000 ft. A 20 arc-second field of view thus corresponds to 1.2 inches in the focal plane. The $f/30$ beam has a small enough included angle so that a Lyot filter may be successfully employed, although it must be emphasized that selection of the optimum means of filtration will warrant careful consideration.

Two problem areas are evident for the system as shown. The first is the high speed and consequent difficulty of manufacture of the secondary and tertiary mirrors. The second is the extreme sensitivity of axial focal position to primary-secondary spacing. With an $f/0.95$ primary mirror and an $f/30$ beam at the focal plane, the lateral and axial magnifications of the secondary optics are $\frac{30}{0.95} = 31.6$ and $(31.6)^2 \approx 1000$, respectively. Hence, a change of 0.1 inch in the primary-secondary spacing will shift the focal plane by 100 inches. It is plain that this sensitivity should be minimized by employing the lowest possible system $f/\text{no.}$ consistent with acceptance angle limitations of the pre-detection filter.

The optical system described resulted from a number of computational cycles and refinements generated with the aid of a high speed computer. The process was terminated when a blur circle diameter of 6 seconds of arc was obtained, since this was considered as adequate demonstration of the inherent feasibility of meeting the specified objectives with a realistic optical system. No inference is intended that the system shown is in any way optimized or even that the basic configuration will prove to be the most advantageous upon more detailed study. It is not improbable, for example, that further refinement could yield reduced curvatures for the secondary and tertiary mirrors.

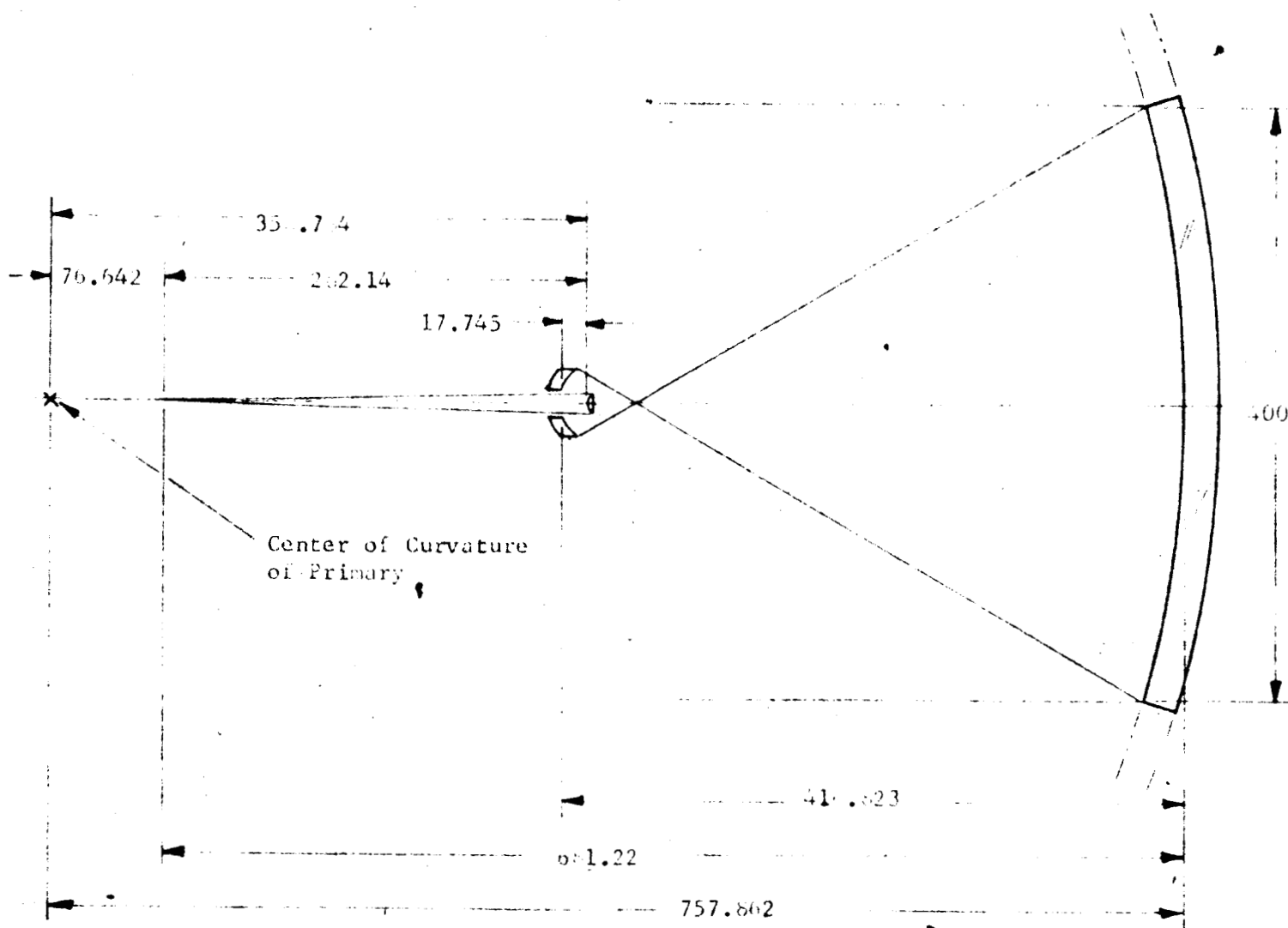
The 6 arc-second blur circle cited above proved to be relatively insensitive to off-axis angles, appreciably greater than those corresponding to a 20 arc-second field-of-view. Hence, any requirement for appreciably larger fields of view, e.g. for acquisition purposes, should not compromise the basic feasibility of the design.

Surface	Radius	Separation	Clear Aperture
1	-757.862 in.	-416.823 in.	400 in.
2	28.72176	17.745	47.6
3	10.9707	-282.14	9.05

Primary f/0.95

EFL = 12000 in. (1/30)

Diameter Circle of Confusion = 6 arc-seconds



Note: Dimensions in inches.

Figure L. Tentative Optical Design

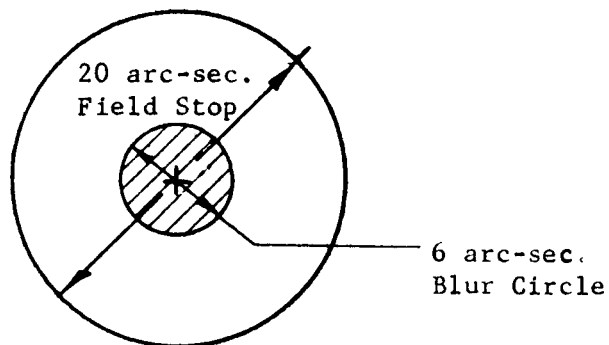
The relationship between field-of-view, blur circle diameter, and misalignments of the primary mirror segments deserves some comment. Figure 16a shows the focal plane of the nominal optical system described above, with a 20 arc-second field stop and an axial blur circle 6 arc-seconds in diameter. This is the result that would be obtained from a perfectly aligned optical system with mathematically correct mirror surfaces. If the primary mirror is to consist of a large number of individual segments and if the arbitrary assumption is made that those segments have randomly oriented tilt errors of 2 arc-seconds, the blur circle diameter grows to approximately 14 arc-seconds as shown in Figure 16b. (Since a 2 arc-second tilt error for a 40-inch diameter segment corresponds to a displacement of only 0.0004 inches across the diameter, it is evident that the assumption is not particularly pessimistic.) It is thus apparent that, with a 14 arc-second diameter blur circle, the energy from a point target will be increasingly vignetted at angles more than 3 arc-seconds off-axis (Figure 16c), and will be completely lost at angles greater than 17 arc-seconds off-axis (Figure 16d). If, for purposes of first-order approximation, we ignore the non-linearities involved, we may plot energy collected versus off-axis angle, as shown in Figure 17. It is evident that the presence of segment tilts decreases the capability of collecting energy from the target and reduces the capability to reject unwanted energy from adjacent sources.

2. Tentative Mechanical Design

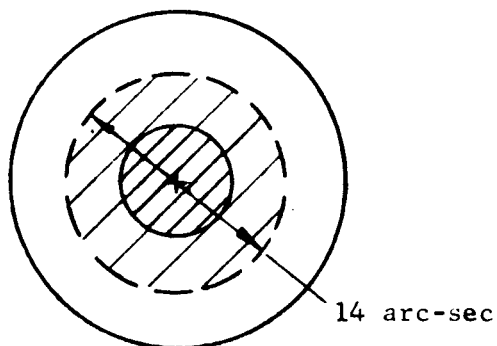
The concepts envisioned for implementation of the fixed-primary system, while by no means worked out in detail, fall generally along the following lines:

Fixed Primary Mirror - The primary mirror, because of its extensive size, would necessarily consist of a number of segments. The most probable shape of these segments is hexagonal, and the most plausible means of producing the required number with the required degree of radius matching is by replication.

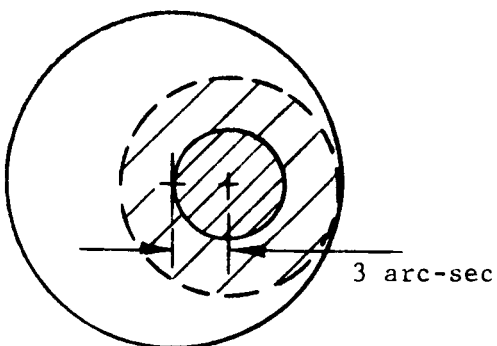
The mirror segments would be supported on rigid pylons by mechanized



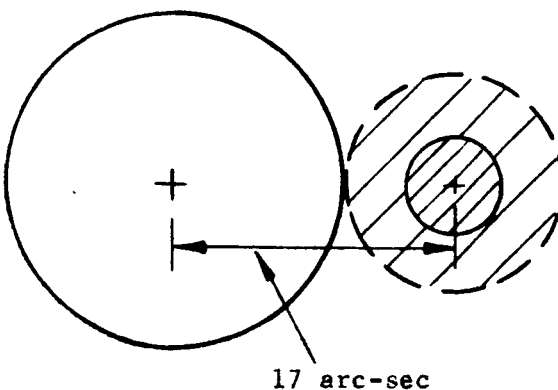
a) On-axis, "Perfect" Primary Mirror



b) On-axis Image, Primary Mirror with Randomly Oriented 2 arc-sec Segment Tilts



c) Maximum Off-axis Angle for no Vignetting



d) Minimum Off-axis Angle for 100% Energy Exclusion

Figure 16. Field Angle Considerations for System with 20 arc-seconds Field Stop, 6 arc-seconds Blur Circle

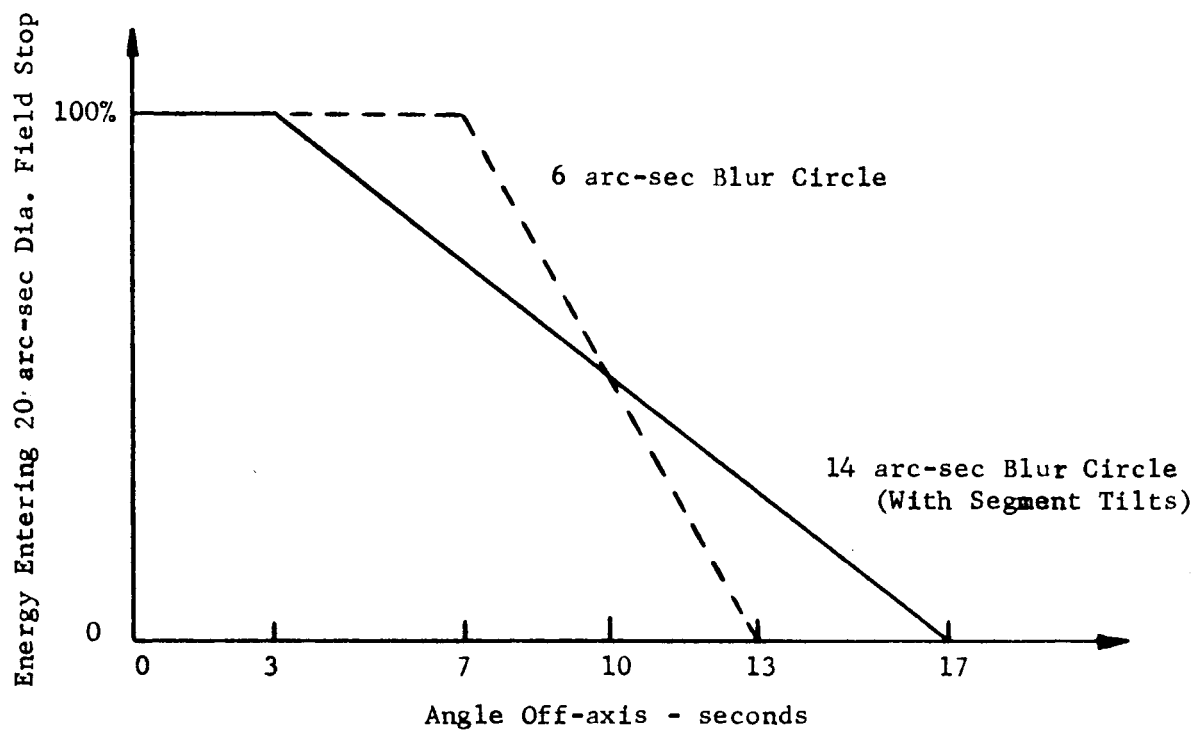


Figure 17. Linear Approximation of Energy Collected vs Angle Off-axis

locating devices augmented by counterweights, or similar force applicators, to whatever degree necessary to maintain the figure of each segment. The locating devices would be operated remotely in conjunction with optical alignment sensors located at the center of curvature of the primary..

The support pylons would be integral with a massive concrete bowl-shaped foundation designed for maximum dimensional stability and providing adequate passageways between the pylons to provide access to the segment support and positioning equipment.

Secondary Optics and Support Structure - A brief survey, sufficient to establish feasibility, has been made of possible approaches to the construction and support of the rotating secondary optics package. The configuration that seems most promising is illustrated by Figure 18.

As indicated, the rotating optical package would consist of a tubular structure somewhat less than 5 feet in diameter and approximately 40 feet long. The secondary and tertiary mirrors at one end of the tube would be counterbalanced at the opposite end in order that the assembly be accurately balanced about a horizontal (elevation) axis passing through the center of curvature of the primary mirrors.

The elevation axis bearings would be supported by an inverted yoke deep enough to clear the aft end of the tube and pivoted about a vertical (azimuth) axis. The azimuth bearings would be contained in a central hub supported by three trusswork beams spanning the primary mirror.

Rough weight estimates and strength computations were performed for the configuration described. The results indicated a total supported weight, including optics, tube, counterweight, elevation axis, yoke, and azimuth hub of 18,000 pounds. This load was imposed on three triangular trusses whose principal members consisted of 4-inch O.D. steel tubes and whose total weight was an additional 13,000 pounds. Rudimentary stress computations indicated maximum truss stresses on the order of 3,000 psi, a value considered sufficiently low to confirm the feasibility of the approach.

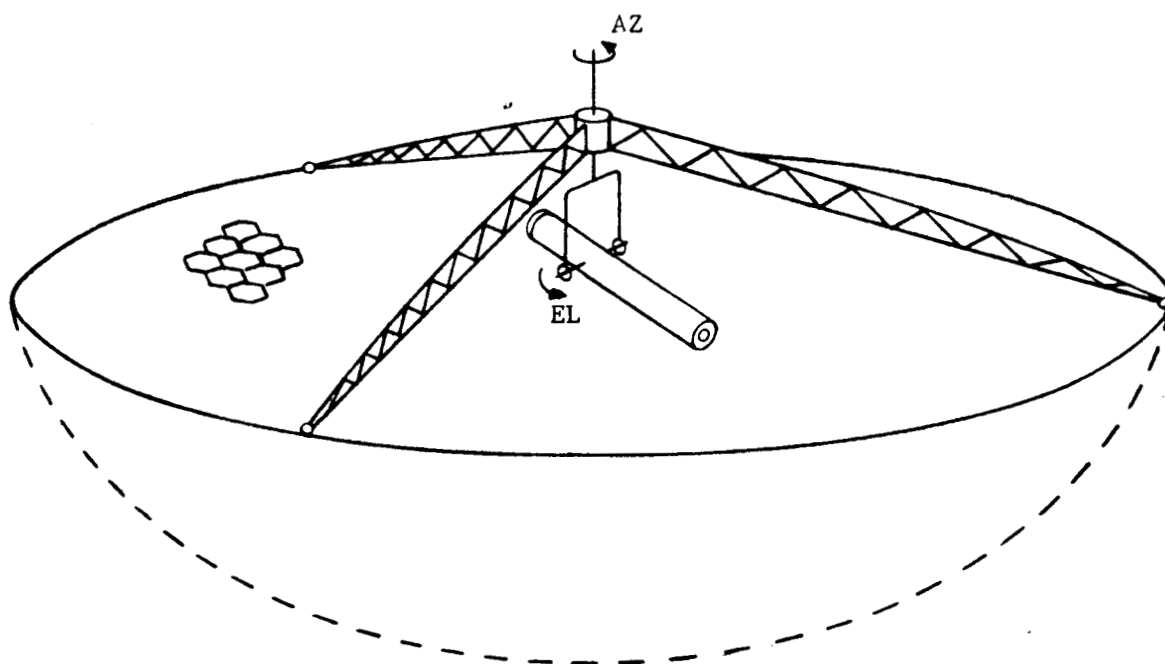


Figure 18. Telescope with Fixed Primary, Alt-azimuth Mounted Secondary Optics

Other combinations of axes are possible for the rotating secondary optics assembly than the alt-azimuth configuration described above. However, the proposed system appears to have enough mechanical and geometrical advantages to warrant its selection over other schemes which might simplify tracking somewhat but which are mechanically cumbersome. An important feature of the alt-azimuth system is the fact that the rotating tube structure and its contents are the only components subjected to varying gravity vectors.

Enclosure - It seems inescapable that an enclosure or dome of some sort over the primary mirror will be mandatory. The three principal functions of such an enclosure would be:

- (1) Protection of the primary mirror from inclement weather and/or wind-borne sand and dust.
- (2) Maintenance of optimum seeing conditions for the instrument.
- (3) Minimization of direct solar thermal inputs.

The first of these items is amenable to straightforward solution, and represents no major problem. The maintenance of proper seeing conditions, however, requires detailed understanding of thermal conditions and air circulation phenomena in and around the instrument and its enclosure. This understanding must include daytime conditions of direct solar radiation, where experience with conventional astronomical instruments is of limited applicability. This is a problem of considerable proportions.

Similarly, direct solar radiation on the primary mirror and/or on the rest of the instrument would almost surely result in unacceptable thermal degradation of the mirror's figure and/or misalignments of the system. The difficulty of avoiding such effects will become acute for targets in proximity to the sun, and will certainly influence the design of the enclosure.

Prognostications of optimum enclosure geometry are of little significance pending intensive study of the entire problem. Possibilities range from a relatively conventional astronomical dome over the entire instrument to individual hinged covers on each primary mirror segment.

Pointing and Tracking Considerations - It is anticipated that the most advantageous approach to the pointing and tracking problem will prove to be an active dual-mode system composed of "coarse" and "fine" controls.

Initial pointing, acquisition, and siderial rate tracking would be accomplished by rotation of the secondary optics package about its azimuth and elevation axes. It is probable that a relatively wide field-of-view would be employed during acquisition in order to minimize the absolute pointing accuracies required, as well as to compensate for residual uncertainties in target position and atmospheric effects.

Following acquisition of the target and initiation of nominal tracking rates by the course drive system, the field-of-view would be narrowed to an optimum value and a fine-guidance mechanism would provide active precision tracking. A likely means of implementing such a fine-guidance system is the inclusion in the optical system of a transfer lens whose lateral position is servo-controlled to maintain the target in the center of the field of view. This approach has been successfully employed in the Stratoscope II balloon-borne telescope. It has the attractive feature of providing fine guidance by controlling a single small element rather than attempting, in the case at hand, to move with extreme precision the massive and relatively unwieldy secondary optics package.

Utilization of the active tracking approach described, desensitizes the system to such persistent problems as varying mechanically or thermally induced deflections in the secondary optics package or its support structure, and fluctuating apparent target location due to atmospheric effects.

C. AZIMUTH-ROTATING PRIMARY MIRROR

The foregoing paragraphs have considered a system whose principal feature is a fixed spherical reflector, chosen primarily as a means of avoiding varying gravity deflections of the mirror and of minimizing the mechanical and structural problems of a very large steerable instrument. As has been

demonstrated, a major shortcoming of such a system is the extensive mirror area required for a system with reasonable sky coverage.

An alternative approach, which buys a major reduction in mirror area requirements at the expense of increased mechanical and structural difficulties, is shown schematically in Figure 19. The mirror is in the shape of a partial spherical zone, the width and length of which are equal to the aperture diameter and determined by the elevation angle coverage required, respectively.

A secondary optics package similar to that described for the fixed primary system rotates about a horizontal (elevation) axis passing through the center of curvature of the primary. The structural requirements for supporting this package are plainly much less demanding than those for the fixed primary mirror approach, since the unsupported span is much shorter.

The entire instrument, including the primary mirror, rotates about a vertical (azimuth) axis. The key feature of this configuration is that rotation of the primary about a vertical axis does not introduce the problem of varying orientations of the mirror with respect to the gravity vector.

With the primary mirror sized to give 90 degrees of elevation angle capability, the telescope provides full coverage of the celestial hemisphere, with no vignetting problems near the horizon, and with no "blind" spots except at zenith, where the maximum angular rate of the azimuth drive would be a limiting parameter. This degree of coverage is an important feature, if maximum versatility and capability of the instrument are desired, and contrasts sharply with the limitations of the fixed mirror concept, where horizon coverage is either absent or gained at considerable additional cost and effort.

The mirror area required for full hemispheric coverage, expressed as a ratio to aperture area, may be shown to be

$$\frac{A_{\text{mirror}}}{A_{\text{aperture}}} = 8 (f/\text{no.}) \left[4 (f/\text{no.}) - \sqrt{16 (f/\text{no.})^2 - 1} + 1/2 \right].$$

8609

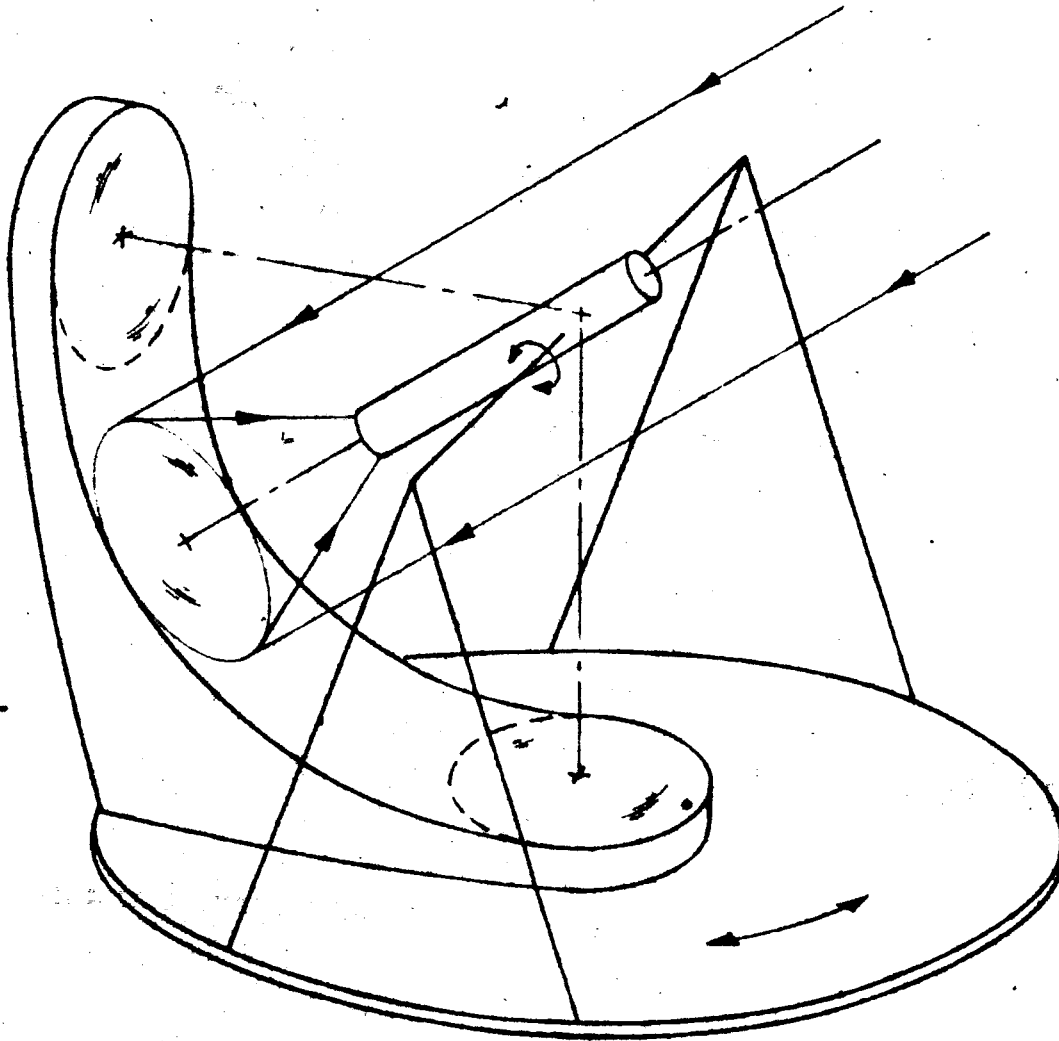


Figure 19. Schematic of Azimuth Rotating Telescope

This relation is shown as the dashed line in Figure 10. The difference in terms of area requirements between this approach and the fixed hemispheric primary (which does not give horizon coverage) is evident, ranging from a factor of 6.4 at $f/1.0$ to a factor of 47 at $f/5.0$. The azimuth-rotating telescope thus enables a major reduction in the cost of the primary mirror segments and their support and positioning hardware.

The obvious drawback, however, is the need for a rotatable mirror support structure of considerable proportions and for a very large azimuth bearing capable of supporting the entire instrument. In neither case does there appear to be any insurmountable technical problem, but particular attention would have to be paid to the thermal and dimensional stability of the support structure. It would seem highly probable that the increased cost and difficulty of a large rotating structure and an appropriate azimuth bearing and drive mechanism are outweighed by the considerable reduction in mirror area and associated mounting hardware; by the obvious attraction of true hemispheric sky coverage; by the relative ease of supporting the secondary optics package; and by the relatively small size of the enclosure required.

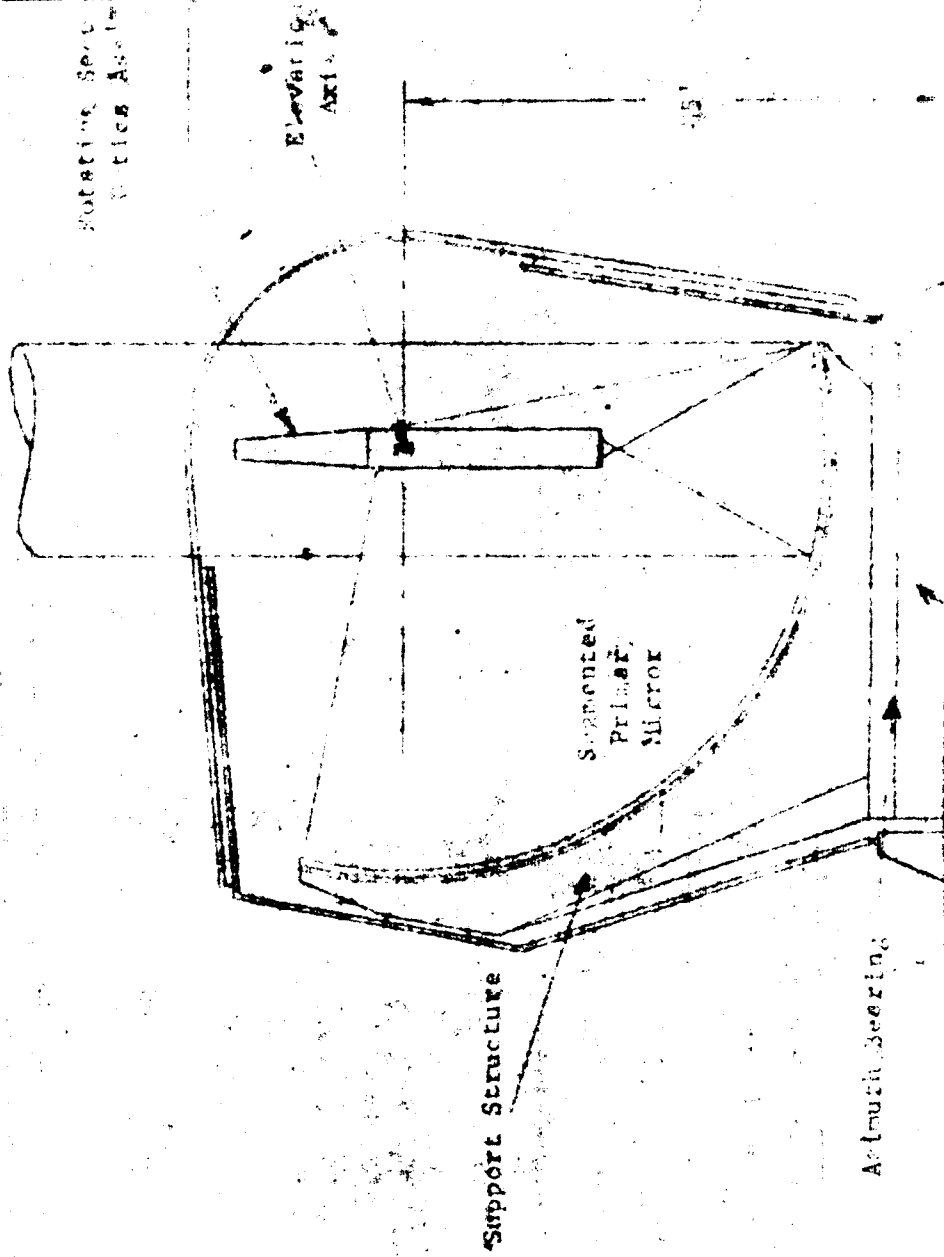
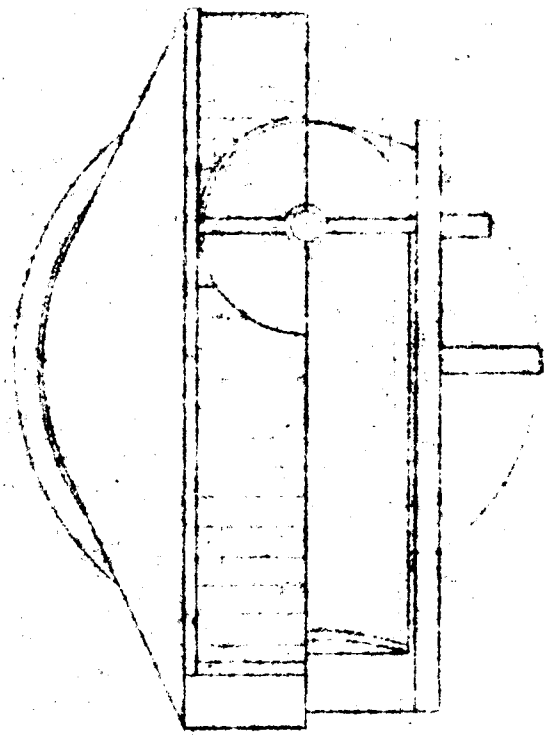
1. Tentative Optical Design

The optical considerations applicable to the azimuth-rotating primary mirror approach are virtually identical with those applicable to the fixed-primary telescope. Hence, the tentative optical design previously described and illustrated in Figure 15 is an appropriate one in this instance as well. Again, no indication is intended that the design shown is in any way optimized, but it may be considered as a demonstration that the desired characteristics can, in fact, be implemented with a realistic optical system.

2. Tentative Mechanical Design

Figure 20 shows a preliminary impression of what an azimuth-rotating telescope with a 10 meter aperture might look like.

As in the fixed mirror approach, the primary mirror would consist of a number of segments, each individually supported and aligned with respect



Elevating Axis

Azimuth Axis

Support Structure

Segmented Primary Mirror

Azimuth Bearing

15'

FIGURE 20. Azimuth Potentiometer Telescope

to a common center of curvature. The segments would be supported by a steel structure configured as shown, designed for maximum rigidity and stability, and providing adequate access to the segments and the support mechanisms. An integral part of the same structure would be a horizontal beam providing support for the elevation bearing and for the rotating secondary optics assembly. The latter would be a cylindrical structure virtually identical to that described for the fixed-primary system.

The entire assembly would be mounted on a circular platform whose principal function would be to distribute loads to the azimuth bearing.

The azimuth bearing presents a challenge if only because of the diameter required (60 to 75 feet for the configuration shown) to impart ample stability to the instrument. The bearing could consist of hydrostatic pads riding on an accurately leveled circular way. Less conventionally, a relatively small-diameter hydrostatic or rolling element bearing could be used to locate the instrument, with the bulk of the static loads carried by floating the instrument in water. In this case, the circular platform comprising the base of the instrument would surmount a circular or annular welded steel float of barge-like construction. This float would be immersed in a water tank or trough to a depth determined to displace most of the weight of the instrument. No more than a few inches of water would be necessary between the float and the tank walls. The result would be a large diameter, very low friction azimuth bearing distributing loads uniformly over a large area but buildable in the field to crude tolerances and with minimal equipment. In addition, it would be relatively insensitive to dimensional changes and soil stability problems. Small changes in water level would permit accurate adjustment to the actual weight of the instrument.

An interesting variation of the concept would be multiple water supports of the sort described, arranged in a concentric tier on the sides of a mound or small hill. This approach would eliminate much of the massive mirror-support structure indicated in Figure 20. It would be essential to maintain constant relative water levels to avoid bending of the structure, but

this should be easy to do with considerable accuracy.

It should be noted that the azimuth bearing axis need not pass through the center of curvature of the primary mirror, but should, in fact pass approximately through the center of gravity of the complete rotating portion of the instrument.

An enclosure of some kind is again a virtual necessity for physical protection from the elements and for proper control of thermal conditions and air circulation. Figure 20 suggests a possible configuration consisting of a slotted housing, which rotates in synchronism with the telescope but is otherwise completely independent of it. Upper and lower rolling doors, reminiscent of a roll-top desk, permit opening of the desired portion of the observing slot.

It may not be necessary to separate the enclosure from the telescope mount. The main purpose in separating them is to insulate the telescope from wind loads and thermal inputs. The image tracking system will have a frequency considerably higher than the natural frequency of the mount. The tracking system will probably be capable of filtering out wind load and thermal disturbances during tracking. It will not, of course, be of help during acquisition. This area will be the subject of further study.

Regardless of the details of the enclosure, the fact that the considerations involved are essentially the same for the fixed primary mirror and for the azimuth-rotating primary mirror concepts should mean that the latter, with its shorter spans and lesser area to be covered, would be simpler and less costly to design and construct.

D. CONVENTIONAL TELESCOPE

A third possible configuration for a giant-aperture optical receiver would be a complete rotatable instrument similar in concept to conventional astronomical telescopes.

As has already been noted, an inevitable problem with such telescopes is the varying orientation of the gravity vector with respect to the primary mirror, and the consequent necessity of virtually eliminating gravity-

induced deflections. A classic example of the required approach to this problem is the complex 36-point counterweight system which supports the 200-inch primary in the Palomar telescope. As has also been noted, the problem would be compounded in a very large aperture system requiring a segmented primary, inasmuch as the virtual elimination of gravity deflections must now be extended to a large positioning structure as well as to the segments themselves.

There are, however, advantages to the approach which warrant careful consideration. The most obvious is the relatively small glass area needed for the primary. The required area is essentially equal to the aperture area instead of 5 times as great for an $f/1.0$ azimuth-rotating system or 32 times as great for an $f/1.0$ hemispherical reflector. It is plain that elimination of that much glass could pay for a lot of counterweights and sophisticated structure!

A second attractive feature of a conventional telescope is the freedom to make the primary mirror a paraboloid or other aspheric, thus avoiding the optically awkward problem of correcting the severe spherical aberrations inherent in the use of a spherical primary.

At this stage of the program, substantial effort has not been devoted to considering the mechanical details of a giant aperture telescope of conventional configuration, since existing experience with large astronomical instruments provides ample background for preliminary evaluation of the concept. It should be apparent, however, that aperture diameters on the order of 10 meters lead inescapably to instruments of mammoth proportions. As a first estimate, a 10 meter telescope of conventional design would correspond to a 2:1 scaling of the 200-inch Palomar installation.

SECTION VI

TELESCOPE CONFIGURATIONS FOR COHERENT DETECTION

A. GENERAL

A very different approach from intensity detection is optical heterodyning or coherent detection.

This technique makes use of local oscillator whose output optical wavefront is combined with the incoming signal wavefront to produce, by beating, an intermediate frequency, which is detected and converted to an electrical signal. Because of the requirement that the wavefronts interfere over substantially all of their areas simultaneously, a stringent requirement put on the entire receiver optical system, including the atmosphere through which the signal passes, is that it distort the geometry of the wavefronts as little as possible.

Except for selecting the best observing sites, elevating the telescope above the surrounding terrain, and providing suitable ground cover at the site, there is little we can do to improve the wavefront disturbing properties of the atmosphere. In view of this, the atmosphere should be made the limiting source of wavefront degradation by having the rest of the optical system of good enough quality to be essentially diffraction limited.

B. FIGURE ACCURACY

An estimate of the figure tolerances required to achieve this may be obtained by applying an equation of Hufnagel and Stanley*. For near perfect systems:

$$M(K) = 1 - \frac{4\pi^2}{\lambda^2} (\bar{\Delta})^2$$

* R.E. Hufnagel and N.R. Stanley, Image Transmission Through Turbulent Media, JOSA 54, 52, 1964.

where

$$\begin{aligned}\lambda &= \text{Wavelength of the light} \\ (\bar{\Delta})^2 &= \text{Mean square deviation of the wavefront} \\ M(K) &= \text{Effective transfer function of the deviations}\end{aligned}$$

The transfer function of a perfect system must be multiplied by $M(K)$ to obtain the most likely transfer function for the imperfect system.

If we set as an objective a transfer function of 0.95 for each element of the system, we find that the mean square wavefront deviation must not exceed

$$\begin{aligned}(\bar{\Delta})^2 &= \frac{\lambda^2 (1 - M(K))}{4\pi^2} = \frac{(1^2) (1 - 0.95)}{4\pi^2} = 0.0013 \\ &= 0.036 \text{ waves}\end{aligned}$$

A mirror surface having a root mean square deviation of 0.018 or 1/55 wave will cause this wavefront deviation. For a 10.6 μ coherent system we require an RMS figure error not exceeding 1/55 λ at 10.6 μ or, stated in the more familiar terms of waves of visible light (5461 \AA) $1/55 \times \frac{10.6}{0.5461} \approx 1/3\lambda$.

An RMS figure accuracy of 1/3 wave would be very easy to obtain, or even exceed, on all elements except the primary mirror. This would present a somewhat more difficult problem for mirrors of 3-4 meter diameter, but is well within the present state of the art.

If we consider a coherent system operating at 4 μ we still have the requirement for 1/50 wave at 4 μ . Converted to the more familiar visible light wavelength we require 1/8 wave. This again presents no problem for the smaller elements and, because the largest coherent aperture that would be used probably would not exceed 2-meters, is perfectly reasonable for the primary.

We can conclude that the figure accuracy attainable on the optical elements at reasonable cost presents no limitation to the coherent system.

C. CONFIGURATION

What would the characteristics of the telescope of a large coherent system be? It would be very similar to a modern astronomical telescope of similar aperture. There appears to be no fundamental reason why an astronomical telescope of suitable aperture could not be used as the receiver for a coherent space communication system, or why, if separate telescopes were constructed for the communication program, they could not be used for astronomical work while not engaged in their prime activity. The optical precision required is commensurate with that found in modern astronomical practice. The mechanical drive precision required is also similar to that required for large astronomical telescopes, although most of these instruments lack the readout equipment and structural stiffness necessary to point to a predetermined area of the sky within a few arc seconds. This does not present a problem for the astronomer, since he has vast numbers of stars of known location to use as a reference.

A wider field of view will be used during acquisition to minimize the absolute pointing accuracy required of the telescope. The field will be reduced during tracking to reduce the noise received from the background.

The coherent receiver will include provision for active tracking of the target, which will increase the effective coherent aperture diameter by reducing the effects of varying wavefront tilt and will reduce the precision required of the main tracking system.

In the case of an equatorial mounting, the course tracking and pointing would be provided by the usual telescope drives, while fine tracking would be obtained by the use of a transfer lens or mirror which would track the image with high precision. The transfer lens servo will have a frequency response of about 20 cps. We estimate that this is high enough to eliminate most of the effect of varying wavefront tilt and also the effects of telescope deflections, drive errors, angular rates different from earth rate, and variation of the refraction angle during the tracking period.

It is possible that an alt-azimuth configuration may be more advantageous than an equatorial mount. In this event, position signals taken from the transfer lens would be used as tracking inputs to the mirror drives.

The tracking and detection optics could probably be located at either the Cassegrain or Coude' focus of the instrument, although this decision would depend on the characteristics of the particular telescope and on the parameters of the tracking and detection system.

We have not studied the coherent telescope configuration in great detail during the first phase of this study, because there do not appear to be any problem areas that cannot be solved by the ordinary engineering techniques. This is not to say that it is a simple project, but rather, that we feel that such a telescope is completely feasible and that most of the likely problems have already been solved during the design of some of the more modern astronomical telescopes.

SECTION VII

CONCLUSIONS AND RECOMMENDATIONS

We feel that either incoherent ground receivers with apertures on the order of ten meters or 10.6 μ region coherent receivers with apertures on the order of four meters are feasible.

The communications aspects discussed in Section II indicate that a 10.6 μ coherent system has several advantages over the short wavelength incoherent systems. The coherence diameter calculations of Section III indicate that coherent apertures of almost four meters are usable day or night. The daytime calculations of Section II are based on a conservative 2 meter aperture. If indeed, four meters can be efficiently used in the daytime, the required laser power outputs would be substantially reduced. The required vehicle pointing accuracy would be substantially easier to attain using 10.6 μ radiation. We must, in making this decision, consider the fact that no 10.6 μ modulator now exists and that further development is required in detector technology and in laser technology. The coherence diameter calculations have areas of uncertainty and should be backed up by measurements in the field.

We feel that for the incoherent 10 meter aperture receiver case the azimuth rotating system shown in Figure 20 is the more fruitful system for further study. Although the large azimuth bearing is a formidable problem in terms of size and cost it is, in our opinion, more than balanced by the substantial reduction in glass area; the smaller and less complex support and drives for the secondary optics; the ease with which protection from weather,

dirt, and direct solar radiation can be provided; and straightforward manner in which hemispheric coverage is achieved. The incoherent system, because of its large aperture, is probably of more interest to astronomers for scientific use when the receiver is not being used for its main purpose as a space communications receiver.

We wish to recommend several areas for study outside the scope of this program. The first of these is directed to short wavelength incoherent systems and the other three are of importance to 10.6μ coherent systems. These are:

1. Investigation of ultra-narrow bandpass predetection optical filters, with emphasis on transmittance, bandpass, thermal and polarization sensitivity. The optical predetection filter preceding the PCM/PL detector in the Earth-based receiver should ideally have a bandwidth equal to the signal bandwidth. However, the narrowest optical filters have a bandwidth which is many orders of magnitude larger than the signal bandwidth. Ultra-narrow Lyot optical filters (less than 1\AA bandpass) may be constructed, but the transmission is quite low, approximately 13%. Since the light input to the Lyot filter must have a single polarization, the PCM/PL receiver is required to have two filters for the two orthogonal polarizations. These filters are also sensitive to small temperature changes.

Recently, filters have been developed which are basically a Fabry-Perot cavity in series with a multilayer filter to suppress the unwanted modes of the cavity. These filters have a bandwidth larger than the Lyot, but the increased temperature tolerance and transmittance of the Fabry-Perot filter

makes them competitive with the Lyot filter.

We note from the data link calculations that the PCM/PL system will be limited by background noise during day operation. This noise source is reduced by inserting an ultra-narrow bandpass optical filter before the detector. For nighttime communications against a star field background, it is possible to widen the predetection filter bandpass and obtain greater transmittance by use of the Fabry-Perot type filters or multilayer filters. However, if nighttime communications with a planetary background (Mars) is considered, then it appears that an ultra-narrow filter must be used.

2. If carbon dioxide lasers are to be employed successfully in deep-space communications systems, it will be important to develop new detector and modulator components specifically adapted to this wavelength region and to the properties of CO₂ lasers. There is a definite need for detectors that reach the theoretical limit of sensitivity, permitting "photon counting" with bandwidths in the tens of megacycles per second or greater. At the present, detectors sensitive at 10.6 μ do not meet these requirements. However, it is believed that this present lack is not based on fundamental physical difficulties. Moreover, it appears to be caused by the fact that until very recently, there could have been no conceivable need for sensitive broadband detectors in this frequency region. In a system where the use of liquid helium cooled detectors is feasible, it will be possible to reach the photon shot noise limit at 10.6 μ . This will require that the detector be suitably shielded from exchanging radiation with its environment except through the solid angle and the wavelength passband through which the signal must come. This means operation of the detector in a cooled reflecting shield, using a cooled narrow passband filter over the signal aperture

Study of the published sensitivities of detectors for the 10μ region shows that signal to noise data reported is not taken while the detector is shielded as described. Noise levels reported for detectors in the 10μ region are generally taken in test setups where the detector exchanges radiation with a field at room temperature through a broad bandwidth. It is suggested that detector experiments be made in test setups that are compatible with the intended use.

It is also true that the structures now available in cooled solid state detectors for this wavelength region have not been specifically engineered to have very broad bandwidths. Again, until very recently it would have been almost impossible to even test the frequency response of a detector in the 50-100 megacycle frequency region using 10.6μ illumination. It appears very definitely that some experimental and theoretical work is necessary to re-measure and re-interpret the performance available from cooled solid state detectors and express it in a form suitable for use in planning an infrared laser communication system. It is clearly necessary to reconfigure, rebuild, and evaluate detectors working on existing principles, to determine at first hand the performance that can be reached in detectors designed for this wavelength band.

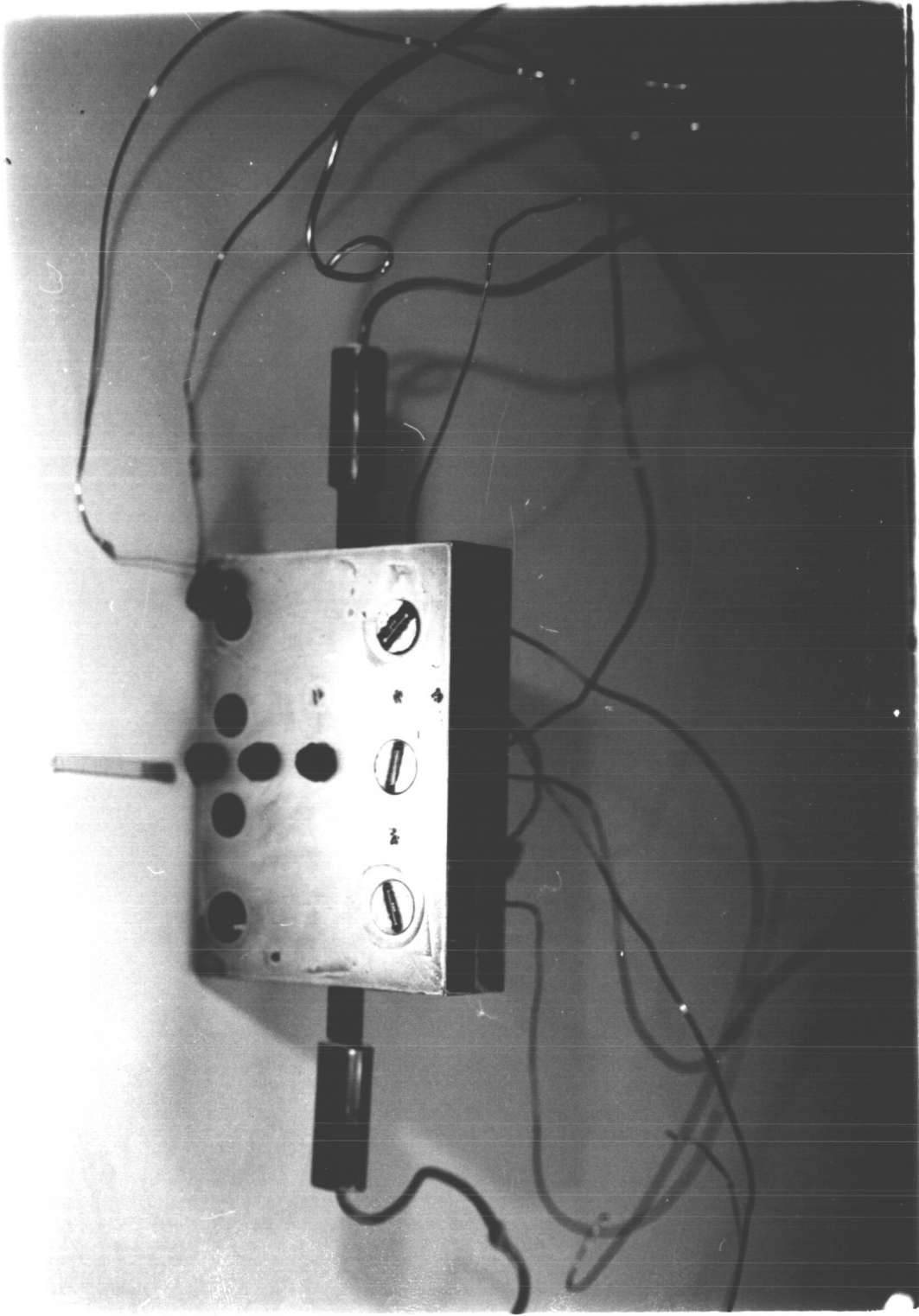
3. An investigation is required to solve the problem of operation of a solid state detector when illuminated by strong local oscillator signal. The impedance level of the detector when illuminated with a laser local oscillator is so different from its dark impedance that the entire detection system must be designed to accommodate this impedance change.

4. It is apparent that theoretical predictions of the lateral coherence diameter for both day and night operation at selected sites must be experimentally verified. The result would be an experimental verification of the validity of extension of propagation theory to the 10μ region. To check the theoretical predictions, it is necessary to plan and execute an experiment using interferometric techniques to measure lateral coherence diameter during day and night at selected sites under different meteorological conditions.

5. A suitable modulator for the 10.6μ region is not now available. This is of course a critical component for a coherent system and should be the subject of a development program. Zinc sulphide is a candidate electro-optical material which is transparent at 10μ . A magneto-optic material, which is also a candidate material, is iron substituted garnet.

We have, in this first phase of the study, pointed out the trade-off that are considered to be important to the selection of ground receivers for deep-space optical communication systems.

We are looking forward to direction from the Jet Propulsion Laboratory in defining the ground receiver systems to be studied in more detail in the second phase of this program.



1. Base Plate with Gauges